

We thank both reviewers for taking the time to review our manuscript and their positive comments. We propose below how we plan to address their comments in revising our manuscript. In the following reviewers comments are indicated in italic font and our response is indicated in bold font.

Reviewer 1

This is a well-written and interesting model description and evaluation of CLASSCTEM. The application of the 1-box model is helpful as a benchmark. I have just a couple of minor comments for helping improve the manuscript.

1. Please mention how the inland water flux is or is not included in the CLASSCTEM wetland emissions estimate, referencing Bastviken, and Thornton GRL where appropriate.

The current CLASS-CTEM modelling framework used in this study does not represent inland lakes. The land mask used by the model is binary with each grid cell either a land or an ocean/water cell. The model is, however, capable of representing inland lakes and in near future this functionality will be represented. We will make this aspect clear in revising our manuscript and also mention the Bastviken and Thornton references.

2. A couple of sentences on how the 1-box model equilibrium is calculated is needed to understand how 708 ppb was estimated. Is there a spinup for this, how many years etc...

No, this process doesn't require any spin up just the application of equations (4) and (5) with dB/dt set to zero. We will explicitly show the calculation of equilibrium 1850 atmospheric methane concentration when revising our manuscript.

3. Does EDGAR 'agricultural soils' include rice cultivation ?

Yes they do. The reason this category was included is because we do not model methane emissions from rice paddies explicitly. We will make this clear in revised manuscript.

4. Main criticism is that the parameter and forcing uncertainties are not explored for CLASS-CTEM. These would affect absolute estimates as well as interannual variability and trends of estimates of CH₄. Some references to ancillary CLASS-CTEM studies on uncertainties would be helpful to address this shortcoming.

This is a valid criticism of any modelling exercise. The CTEM (i.e. biogeochemical) part of the CLASS-CTEM model has more than 100 model parameters alone. While several aspects of the model have been evaluated in the past at point, regional, and global scales a comprehensive sensitivity analysis is beyond the scope of this study. We will, however, include a discussion of uncertainties related to parameters that determine wetland extent and methane emissions from wetland and fire including those that affect the trend of wetland methane emissions.

Reviewer 2

The manuscript deals with an assessment of natural methane emission from wetlands and fire and soil uptake simulated by a one box model. The paper contains some interesting material, is reasonably well written and is generally well referenced. But the number of figures and tables is too high, some figures should be moved to the Supplement. In summary, the manuscript might be published after major revision.

Thank you for your comments. We will reduce the number of figures and following your suggestion move some material to an appendix or supplementary information.

Specific comments Line 41 - : : reasonably well with observation based estimates. Could you give any estimations for errors and obtained methane emissions in the Abstract.

We will mention the relevant primary numbers for atmospheric methane concentration and wetland methane emissions in the abstract when revising our manuscript.

Line 58-80 – Remove. Contents is not typical for research article.

Thank you for noticing. Yes, of course, we will delete the Contents. These were put in for ease of the reviewers.

Line 88, 91,94 etc – Remove brackets at [CO₂].

The word CO₂ or CH₄ in square brackets is meant to represent atmospheric CO₂ or CH₄ concentration. We will check with the copy editing office to ensure if it is acceptable to use this format.

Line 98 – Give a reference to a paper where CH₄ concentration values were obtained.

We will include the Prather et al. (2012) reference for the methane concentration values when revising our manuscript.

Line 100 – Global warming potential usually is calculated over a specific time interval. According to IPCC 2013 CH₄ GWP is 7.6 – 72 times higher than CO₂ GWP, and other GHG (N₂O, CF₄, HFC-134a) have higher GWP than CH₄.

Thank you for providing this information. We will include this information and the IPCC reference when revising our manuscript.

Line 199 – CLASS model calculates the energy and water balance according to four PFT. None of them is related to wetlands. Is it correct to use upland vegetation types to simulate wetlands?

Thank you for raising this interesting question. It is correct that CLASS-CTEM model does not include any wetlands specific vegetation types. However, as argued in section 2.1.1.2 at large spatial scales the dominant controls on wetland methane emissions are temperature, wetland extent, and available substrate for decomposition. At large spatial scales both net primary productivity and heterotrophic respiration are determined by climate. This is the reason why models

like the Miami model which only use mean annual temperature and precipitation are able to reasonably reproduce the spatial distribution of net primary productivity at the global scale. For the same reason, the CLASS-CTEM model is able to simulate spatial distribution of methane emissions reasonably as long as the spatial distribution of net primary productivity and heterotrophic respiration is reasonable. The corollary of this is that the model will not be able to reproduce methane emissions at a point scale for wetlands and peatlands as reliably as it does at large spatial scales. We will include additional discussion around this aspect when revising our manuscript.

Line 243 -256 – Conception of seasonal changes in wetland extent needs more explanation. Wetland is a land area that is saturated with water (seasonally or permanently). According to figure 14a there is no wetlands in WSL in winter. It is not true. Seasonally frozen and covered by snow wetlands are still act as a source of methane (Langer et al., Biogeosciences, 12, 977-990, 2015 ; Korkiakoski et al, Biogeosciences, 14, 1947–1967, 2017). Details about wetland fraction computation and Table 1 can be moved to Supplementary.

While it is true that wetlands are capable of producing small methane emissions during the winter when they are frozen it is still unclear how much do these emissions contribute to the annual total. As seen in Figure 14 most models and even inversion-based estimates show very little emissions during the winter season when wetlands are frozen. We have some discussion around this aspect on page 37 of the existing manuscript and we will expand it more. We will also move details about wetland fraction computation and Table 1 to an appendix or supplementary information.

Line 296 – Function regulating emission with soil moisture change should be evaluated in details. Melton et al. (2015) describe basic and alternative types of dependences of CO₂ heterotrophic respiration from soil moisture. Please give some proofs of applicability this kind of model for CH₄ emission.

The basic premise of the dependence of heterotrophic respiration on soil moisture is that heterotrophic respiration is reduced at both too high and too low soil moistures. It is in between these extremes that heterotrophic respiration is at its highest. When soils are saturated and water table is above the surface then respiration is reduced due to lack of available oxygen for the microbes. The modeling approach that we have used further reduces heterotrophic respiration calculated by the CO₂ module of the model by multiplying it with 0.45 to account for this decrease due to anaerobic respiration. In the absence of evaluation of methane emissions at a point scale we can only use this conceptual basis to justify the applicability of our approach. We realize that this is a limitation and we will make a note of this when revising our manuscript.

Line 670-675 – Changes in methane emission from rice paddies due to land use changes and rapid agricultural development in East Asia should be mentioned.

Yes it is true that increasing methane emissions from rice paddies and agricultural development in East Asia have contributed to increase in atmospheric methane concentration. In our modeling study, this increase comes from the specification of anthropogenic methane emissions from the RCP and EDGAR

data sets through the agricultural emissions category. Note that the model does not simulate emissions from rice paddies and so their specification is important. We will make this point clear when revising our manuscript.

Figures 1,2,7,8 can be abandoned or moved to Supplementary.

Figures 5,9,15 (also 6,10) can be joined in to two charts.

We will combine figures and move them to an appendix or supplementary information as suggested to reduce the total number of figures when revising our manuscript.

1 Dear Editor,
2
3 We have revised our manuscript following reviewers' comments as we outlined in our posted
4 response.
5
6 We have reduced the number of figures from 15 to 10 by moving 5 figures into appendices
7 including the section about calculation of wetland extent.
8
9 Changes to our manuscript are tracked and shown below.
10
11 Thanks,
12 Vivek.
13
14
15

16
17
18
19
20
21
22
23
24
25
26
27 **An assessment of natural methane fluxes simulated by the**
28 **CLASS-CTEM model**

29
30 Vivek K. Arora¹, Joe R. Melton², and David Plummer¹.
31

32 ¹Canadian Centre for Climate Modelling and Analysis, Environment and Climate Change Canada,
33 University of Victoria, Victoria, B.C., V8W 2Y2, Canada
34
35

36 ²Climate Research Division, Environment and Climate Change Canada,
37 Victoria, B.C., Canada
38
39
40
41

Abstract

Natural methane emissions from wetlands and fire, and soil uptake of methane, simulated using the Canadian Land Surface Scheme and Canadian Terrestrial Ecosystem (CLASS-CTEM) modelling framework, over the historical 1850-2008 period, are assessed by using a one box model of atmospheric methane burden. This one box model also requires anthropogenic emissions and the methane sink in the atmosphere to simulate the historical evolution of global methane burden. For this purpose, global anthropogenic methane emissions for the period 1850-2008 were reconstructed based on the harmonized representative concentration pathway (RCP) and Emission Database for Global Atmospheric Research (EDGAR) data sets. The methane sink in the atmosphere is represented using bias-corrected methane lifetimes from the Canadian Middle Atmosphere Model (CMAM). The resulting evolution of atmospheric methane concentration over the historical period compares reasonably well with observation-based estimates (correlation=0.99, root mean square error = 35 ppb). The modelled natural emissions are also assessed using an inverse procedure where the methane lifetimes required to reproduce the observed year-to-year increase in atmospheric methane burden are calculated based upon the global anthropogenic and modelled natural emissions that we have used here. These calculated methane lifetimes over the historical period fall within the uncertainty range of observation-based estimates. The present-day (2000-2008) values of modelled methane emissions from wetlands (169 Tg CH₄/yr) and fire (27 Tg CH₄/yr), methane uptake by soil (29 Tg CH₄/yr), and the budget terms associated with overall anthropogenic and natural emissions are consistent with estimates reported in a recent global methane budget that is based on top-down approaches constrained by observed atmospheric methane burden. The modelled wetland emissions increase over the historical period in response to both increase in precipitation and increase in atmospheric CO₂ concentration. This increase in wetland emissions over the historical period yields evolution of the atmospheric methane concentration that compares better with observation-based values than the case when wetland emissions are held constant over the historical period.

Deleted: observed

Formatted: Subscript

1. Introduction

Earth system models (ESMs) represent physical climate system processes and their interactions with biogeochemical processes focusing primarily on the carbon cycle in the context of carbon dioxide (CO₂). These models are able to project how the atmospheric concentration of carbon dioxide ([CO₂]) will change in response to changes in anthropogenic CO₂ emissions or alternatively diagnose anthropogenic CO₂ emissions required to achieve a specific CO₂ concentration pathway (Jones et al., 2013). This capability is achieved by modelling [CO₂] as a prognostic variable which itself requires modelling of the surface-atmosphere exchange of CO₂ and hence the need for land and oceanic carbon cycle components in ESMs (Arora et al. 2013; Friedlingstein et al. 2006; Friedlingstein et al. 2014). While most ESMs include the capability of modelling [CO₂] as a prognostic variable there are only a handful of ESMs which are beginning to treat the atmospheric concentration of methane, ([CH₄]), as a fully prognostic variable (Collins et al., 2011; Shindell et al., 2013).

The [CH₄] has increased from 700 ± 25 ppb in 1750 to 1795 ± 18 ppb in 2010 (Prather et al., 2012). The [CO₂] has increased globally from 278 (276–280) ppm in 1750 to 390.5 (390.3–390.7) ppm in 2011. The greater global warming potential of CH₄ compared to CO₂ (84 and 28 for 20-years and 100-year time scales, respectively), has made methane the second most radiatively important greenhouse gas (GHG) after carbon dioxide CO₂ (Myhre et al., 2013).

The CO₂ radiative forcing for the period 1750–2011 is 1.82 W/m² (associated with ~112 ppm increase), while the radiative forcing for CH₄ over the same period is 0.48 W/m² (associated with ~1081 ppb = 1.08 ppm increase) (Myhre et al., 2013). Since methane is a short-lived GHG with an atmospheric lifetime of around 9 years (compared to CO₂ which has an atmospheric lifetime of around 100–200 years), mitigation of anthropogenic CH₄ emissions

Deleted: 22

Deleted: 1803

Deleted: 2

Deleted: 2011

Formatted: Font: (Default) Times New Roman, 12 pt

Field Code Changed

104 can lead to a decrease in its atmospheric concentration within a timeframe of 10-20 years. As
105 a result methane is considered a short-lived climate forcer (SLCF) and therefore reduction in
106 its anthropogenic emissions offers an attractive and potentially viable target for short-term
107 climate change mitigation policies (Shindell et al., 2012). To be able to address climate
108 benefits of reduction in anthropogenic CH₄ emissions within the framework of
109 comprehensive ESMs, however, it is necessary to model [CH₄] as a prognostic variable in
110 these models.

111

112 Treatment of [CH₄] as a fully prognostic variable in ESMs is hindered by at least two factors.

113 First, the global CH₄ budget is not as well understood as for CO₂. Our lack of ability to close
114 the present-day global CH₄ budget is illustrated in Saunio et al. (2016) who present a recent
115 synthesis of several studies and summarize the present-day global CH₄ budget. Saunio et al.

Field Code Changed

Field Code Changed

116 (2016) show a large discrepancy between total CH₄ emissions, from both anthropogenic and
117 natural sources, for the 2003-2012 period as inferred from the top-down atmospheric
118 inversion-based approaches (558 Tg CH₄/yr) and those based on bottom-up modelling and
119 other approaches (736 Tg CH₄/yr). The primary reason for this discrepancy is that there are
120 multiple sources of both natural and anthropogenic CH₄ emissions so the bottom-up
121 approaches that add up all the individual sources inevitably give larger total emissions than
122 top-down approaches that are constrained by the atmospheric CH₄ burden and its loss in the
123 atmosphere. Second, unlike CO₂, CH₄ has a sink in the atmosphere which requires
124 representation of atmospheric chemistry in ESMs to properly account for the removal of CH₄
125 and feedbacks of methane on chemistry. CH₄ is destroyed in the troposphere and stratosphere
126 due to its reaction with OH radicals and chlorine. This is typically very computationally
127 expensive to represent. As an example, the model years per wall clock day simulated by [the](#)
128 [atmospheric component of the](#) second generation Canadian Earth System Model (CanESM2;

129 Arora et al., 2011) are reduced by a factor of around six when atmospheric chemistry is
130 turned on.

131
132 Despite these two challenges there are ways forward to model [CH₄] as a fully prognostic
133 variable and be able to use comprehensive ESMs to ask questions that the climate modelling
134 community has asked so far in the context of CO₂. For example, how would future [CH₄]
135 change in response to changes in anthropogenic and natural CH₄ emissions, or alternatively
136 what should anthropogenic CH₄ emissions be to achieve a given CH₄ concentration pathway,
137 all while as anthropogenic CO₂ emissions continue to increase? In terms of emissions, since
138 the top-down estimates of CH₄ emissions from natural and anthropogenic sources are better
139 constrained than the bottom-up estimates they are likely to provide more robust estimates for
140 evaluating ESMs and their CH₄ related components. The expensive atmospheric chemistry
141 modules can be replaced with simple first-order representations of chemical losses or,
142 ignoring the spatial variations in CH₄ concentration, the global average concentration of
143 methane can be simulated with a box model using specified methane life times which are
144 calculated a priori using full 3D chemistry-climate models. Although, of course, using
145 specified CH₄ losses implies that feedbacks of methane on methane loss rates and interactions
146 between atmospheric chemistry and climate can be neglected.

147
148 The CLASS-CTEM modelling framework serves as the land surface component in the family
149 of Canadian ESMs (CanESMs) (Arora et al., 2009, 2011; Arora and Scinocca, 2016)
150 developed by the Department of Environment and Climate Change, Government of Canada,
151 and models the land-atmosphere fluxes of water, energy and CO₂. It consists of the Canadian
152 Land Surface Scheme (CLASS) and the Canadian Terrestrial Ecosystem Model (CTEM). In
153 preparation for modelling [CH₄] as a prognostic variable in future versions of CanESMs we

154 have included several CH₄ related processes in the CLASS-CTEM modelling framework.
155 These include representations of dynamic natural wetlands and their CH₄ emissions, CH₄
156 emissions from fires, and uptake of CH₄ by soils. This paper evaluates the simulated spatial
157 distribution of wetlands as well as the magnitude of CH₄ emissions from wetlands and fires,
158 and CH₄ uptake by soils against their respective present-day observation-based estimates. We
159 also evaluate the simulated time evolution of the global sums of these fluxes for the 1850-
160 2008 period by using a one-box model of atmospheric CH₄ burden. This one-box model
161 requires anthropogenic CH₄ emissions, emissions from other natural sources that aren't
162 modelled in the CLASS-CTEM framework, and a representation of atmospheric sinks. The
163 anthropogenic CH₄ emissions for the period 1850-2008 are obtained by harmonizing the RCP
164 and EDGAR data sets, and natural emissions from sources that aren't modelled are specified.
165 Finally, the atmospheric sink of CH₄ is based on bias-corrected global atmospheric lifetime of
166 CH₄ as computed by the Canadian Middle Atmosphere Model (CMAM). The one-box model
167 of atmospheric CH₄ burden is used to evaluate CLASS-CTEM simulated natural CH₄ fluxes
168 by comparing simulated evolution of global [CH₄] with their observation-based estimates as
169 well as by comparing the CH₄ lifetime required to reproduce the observed evolution of global
170 [CH₄] over the historical period with their observation-based estimates.

171
172 The rest of this paper is organized as follows. A brief description of the CLASS-CTEM
173 modelling framework is presented in Section 2 along with the details of methane related
174 processes that are implemented, the data sets used and the experimental protocol. Results are
175 presented in Section 3 and finally discussion and conclusions are presented in Section 4.

176 **2. Model, data and experimental set up**

177 **2.1 The CLASS-CTEM model and its forcing and evaluation data sets**

178 **2.1.1 The CLASS-CTEM model**

179
180 The CLASS-CTEM modelling framework consists of the Canadian Land Surface Scheme
181 (CLASS) and the Canadian Terrestrial Ecosystem Model (CTEM) which are coupled to each
182 other and which together simulate fluxes of energy, water, CO₂ and now CH₄ at the land-
183 atmosphere boundary. Together, CLASS and CTEM form the land surface component in
184 Canadian Earth System Models - CanESM1 (Arora et al., 2009), CanESM2 (Arora et al.,
185 2011), and CanESM4.2 (Arora and Scinocca, 2016).

186
187 CLASS simulates atmosphere-land fluxes of energy and water and it prognostically
188 calculates the liquid and frozen soil moisture contents, and soil temperature for its soil layers,
189 the liquid and frozen moisture contents and temperature of the single vegetation canopy layer
190 (if present) and the snow water equivalent and temperature of a single snow layer (if present).
191 CLASS is described in detail in Verseghy (1991), Verseghy et al. (1993) and Verseghy
192 (2000). In the version 3.6 of CLASS used here, the thicknesses of the three permeable soil
193 layers are specified as 0.1, 0.25 and 3.75 m, although the model can be configured to use any
194 number of layers with specified thicknesses. The thicknesses of the permeable layers also
195 depend on the depth to the bedrock which is specified on the basis of the global data set of
196 (Zobler, 1986). For example, if the depth to bedrock is only 2 m, then the thicknesses of the
197 permeable soil layers are taken to be 0.1, 0.25 and 1.65 m. The energy and water balance
198 calculations are performed for four plant functional types (PFTs) (needleleaf trees, broadleaf
199 trees, crops and grasses). CLASS operates at a sub-daily time step and a time step of 30
200 minutes is used here.

201

CTEM simulates the fluxes of CO₂ at the land-atmosphere boundary and in doing so models vegetation as a dynamic component of the climate system. It models photosynthesis, autotrophic respiratory fluxes from its three living vegetation components (leaves, stem and roots, denoted respectively by L, S and R) and heterotrophic respiratory fluxes from its two dead carbon components (litter and soil carbon, denoted respectively by D and H). The flow of carbon through these five carbon pools is explicitly tracked which allows to calculate the amount of carbon in these pools as prognostic variables. Disturbance through fire and land use change are also modelled. CTEM cannot operate without coupling to CLASS. Its photosynthesis module operates at the same time step as CLASS and requires estimates of net radiation and soil moisture from CLASS. In return, CTEM provides CLASS with dynamically simulated structural attributes of vegetation which are functions of the driving meteorological data. The amount of carbon in the leaves, stem and root components is used to estimate structural attributes of vegetation. The leaf area index (LAI) is calculated from leaf biomass using PFT-dependent specific leaf area (SLA, m²/Kg C) which determines the area of leaves that can be constructed per unit leaf carbon biomass (Arora and Boer, 2005a); vegetation height is calculated based on stem biomass for tree PFTs and LAI for grass PFTs (Arora and Boer, 2005a); and rooting depth is calculated based on root biomass (Arora and Boer, 2003). Other than photosynthesis, all terrestrial ecosystem processes in CTEM are modelled at a daily time step. CTEM models its terrestrial ecosystem processes for nine PFTs that map directly to the PFTs used by CLASS. Needleleaf trees in CTEM are divided into deciduous and evergreen for which terrestrial ecosystem processes are modelled separately, broadleaf trees are divided into cold and drought deciduous and evergreen types, and crops and grasses are divided into C₃ and C₄ versions based on their photosynthetic pathways. The version 2.0 of the model is explained in detail in Melton and Arora (2016), while version 2.1

Field Code Changed

Field Code Changed

226 is used here which amongst other minor changes includes all methane related processes
227 discussed below.

228
229 The methane related processes implemented in CLASS-CTEM build on the model's existing
230 capabilities. Processes are implemented to be able to dynamically model the geographical
231 distribution of wetlands and their methane emissions, methane emissions from fire and
232 methane uptake by upland soils. The fractional coverage of wetlands in a grid cell is based on
233 flat fraction within a grid cell with slope less than 0.2% and grid-averaged soil moisture. The
234 methodology is explained in Appendix A.

235 2.1.1.1 Wetland methane emissions

236
237 The dominant controls on methane emissions in nature are considered to be 1) the position of
238 the water table below which methane is produced due to anoxic decomposition of available
239 organic matter and above which methane is oxidized, 2) the soil temperature which
240 determines the rate of decomposition of organic matter, 3) the availability of organic matter
241 itself, and 4) the pathway through which methane is transferred to the atmosphere (through
242 soil via molecular diffusion, through stems of the vascular plants and through ebullition if the
243 water table is above the soil surface). These factors are not completely independent and their
244 relative importance changes as environmental conditions change (Walter and Heimann,
245 2000). The explicit consideration of these factors becomes more important as the spatial
246 scale at which CH₄ emissions are being modelled reduces. For example, Zhu et al. (2014b)
247 show that as the modelling spatial scale reduces from 100 to 5 km, the dominant control on
248 simulated wetland CH₄ emissions switches from soil temperature to water table depth.

249

Formatted: Normal, Justified, Line
spacing: Double

Deleted: ¶
2.1.1.1 Wetland extent¶

¶
The distribution of wetlands is based on simple formulation which takes into account the topography in a grid cell and simulated grid-averaged soil moisture content similar to Kaplan (2002). The ETOPO1 digital elevation data (Amante and Eakins, 2009) are used to calculate slopes at 1 arc minute (1/60th degree) resolution. Each 1 arc minute grid cell is assigned a slope that is the average of eight slopes based on its elevation and the elevation of its eight surrounding grid cells. The objective is to find what fraction of a grid cell, at some given resolution, has slopes flatter than a given slope threshold. Figure 1 displays the fraction of each 0.5 degree grid cell with slopes less than the threshold of 0.002 (i.e. 0.2% slope) calculated using 1 arc minute slopes, hereafter referred to as the "flat" fraction of a grid cell (f_s). The flat fraction of grid cells is also shown at the current operational 2.81° resolution of CanESM4.2, which is the spatial resolution we have used in this study. Figure 1 shows that the approach is able to identify the flat regions of the world including the West Siberian and Hudson Bay lowlands, parts of northern Africa and in South America the Pantanal and the region bordering Argentina, Paraguay and Uruguay.¶

¶
The flat fraction is the maximum fraction of a grid cell that can potentially become a wetland, if soils are sufficiently wet, and thus a source of CH₄ emissions. As the grid-averaged simulated soil wetness (w_s) the top soil layer increases, above a given lower threshold (w_{low}) in a grid cell, its wetland fraction (f_w) is assumed to increase linearly until some specified higher soil wetness threshold (w_{high}) up to a maximum value equal to the flat fraction (f_s) in a grid cell.¶

$$f_w = \max \left(0, \min \left(f_s, \left(\frac{w - w_{low}}{w_{high} - w_{low}} \right) f_s \right) \right) \quad (1)$$

¶
Soil wetness ($w = \frac{\theta - \theta_p}{\theta_l - \theta_p}$) itself is defined as the ratio of volumetric liquid soil moisture content (θ_l) to the soil

Moved down [2]: 2.1.1.1 Wetland

¶
The distribution of wetlands is based on simple formulation which takes into account the topography in a grid cell and simulated grid-averaged soil moisture content similar to Kaplan (2002). The ETOPO1 digital elevation data (Amante and Eakins, 2009) are used to calculate slopes at 1 arc minute (1/60th degree) resolution. Each 1 arc minute grid cell is assigned a slope that is the average of eight slopes based on its elevation and the elevation of its eight surrounding grid cells.

Deleted: 2

Field Code Changed

At the current operational resolution of around 2.81° of CanESM (equal to about 310 km at the equator) we expect dominant controls on methane emissions to be soil moisture, soil temperature and the availability of organic matter and this allows us to use the simple approach that we have used here. This approach also allows us to estimate CH₄ emissions from wetlands without the use of wetland specific PFTs since at large spatial scales net primary productivity (NPP) and heterotrophic respiration are governed by climate (Chengjin et al., 2016). CH₄ emissions are simulated to occur over the wetland fraction of the grid cell. The simulated CH₄ emissions from wetlands are calculated by scaling the heterotrophic respiratory flux (R_h) from model's litter (D) and soil (H) carbon pools which itself depends on soil temperature, soil moisture, and the available organic matter. Heterotrophic respiration from the litter and soil carbon pools takes the following basic form, with the formulation explained in detail in Melton and Arora (2016)

$$R_{h,i} = 2.64 \times 10^{-6} \zeta_i C_i f_i(Q_{10}) f_i(\Psi), i = D, H$$

$$R_h = R_{h,D} + R_{h,H}$$

where ζ_i represents the base respiration rate (kg C (kg C)⁻¹ year⁻¹) at 15°C, C_i is the amount of carbon in model's litter or soil carbon pool (kg C m⁻²), $f_i(Q_{10}) = Q_{10}^{0.1(T_i-15)}$ is a Q_{10} function that models the effect of temperature, T_i is the temperature of litter or soil carbon pool (°C) and $f_i(\Psi)$ is the function that reduces heterotrophic respiration when soils are too dry and too wet using the soil matric potential (Ψ) (Melton et al., 2015). The constant 2.64 × 10⁻⁶ converts units from kg C m⁻² yr⁻¹ to mol CO₂ m⁻² s⁻¹.

Modelled CH₄ emissions from wetlands, per unit area of a grid cell (mol CH₄ m⁻² s⁻¹), are calculated as

Formatted: Font: (Default) Times New Roman, 12 pt

Deleted: 2

472

473

$$E_w = R_h f_w \alpha_w \delta_s$$

(2)

Deleted: 3

474

475 where f_w is the wetland fraction in a grid cell mentioned above, α_w is the ratio of wetland to
476 upland heterotrophic respiratory flux, and δ_s converts flux from CO_2 to CH_4 units but also
477 takes into account that some of the CH_4 flux is oxidized in the soil column before reaching
478 the atmosphere. A value of 0.45 is used for α_w since heterotrophic CO_2 respiratory flux over
479 lowlands is typically lower than over uplands due to limitation by increased soil moisture
480 including a high water table level. While the $f_i(\Psi)$ function in equation (1) does reduce
481 heterotrophic respiration when soils are wet it does so using only the grid averaged soil
482 moisture content. Wania et al. (2010) use a preferred value of δ_s equal to 0.1 and Zhu et al.
483 (2014a) found δ_s varies between 0.1 and 0.7 with a mean value of 0.23 when calibrating
484 their model against data from 19 sites. A value of 0.135 is used for δ_s in this study. The
485 product $\alpha_w \delta_s$ thus equals 0.061 which implies that for each $\text{mol CO}_2 \text{ m}^{-2} \text{ s}^{-1}$ of heterotrophic
486 respiratory flux $0.061 \text{ mol CH}_4 \text{ m}^{-2} \text{ s}^{-1}$ is generated over unit area that is deemed wetland. At
487 large spatial scales CH_4 and CO_2 heterotrophic respiratory fluxes are expected to be highly
488 correlated since to the first order they are both governed by temperature and the amount of
489 organic matter available for decomposition (Dalva et al., 2001; Zhu et al., 2014a). In addition,
490 as the spatial scale increases it is possible to ignore the effect of water table depth as Zhu et
491 al. (2014b) illustrate.

Field Code Changed

Field Code Changed

Field Code Changed

492

2.1.1.2 Fire methane emissions

Deleted: 3

493

494 Fire in CLASS-CTEM is modelled using an intermediate complexity scheme, which
495 represents both natural and human-caused fires, and accounts for all elements of the fire

triangle: fuel load, combustibility of fuel, and availability of ignition sources. The fire module accounts for both natural fires caused by lightning and anthropogenic fires which are the result of ignitions caused by humans expressed as a function of population density. Increasing population density increases human-caused fire ignitions but also increases suppression of fire. The suppression of fire represents fire-fighting efforts, landscape fragmentation and other processes which leads to a reduction in area burned and is also modelled as a function of population density. The original fire parametrization is described in Arora and Boer (2005b) which has since been adapted and used in several other DGVMs (Kloster et al., 2010; Li et al., 2012; Migliavacca et al., 2013). The fire module in CTEM v. 2.1 incorporates changes suggested in these studies as well as several new improvements which are summarized in detail in Melton and Arora (2016). The approach has been evaluated at the global scale in Arora and Melton (2018) who assess how reduction in global wildfire emissions since 1930s leads to an enhanced land carbon sink. The two primary outputs from the fire module are fraction of area burned per grid cell and dry organic biomass burned per unit area (gC m^{-2}). The dry organic matter burned is then multiplied by corresponding emissions factors to obtained emissions (g species m^{-2}) for several species of trace gases and aerosols including methane (CO_2 , CO , CH_4 , H_2 , NH_3 , NO_x , N_2O , total particulate matter, particulate matter less than $2.5 \mu\text{m}$ in diameter, and black and organic carbon). These emissions factors are based on an updated set by Andreae and Merlet (2001) listed in Tables 3 and 4 of Li et al. (2012).

Field Code Changed

Field Code Changed

Formatted: Font: (Default) Times New Roman, 12 pt

Formatted: Font: (Default) Times New Roman, 12 pt

2.1.1.3 Soil uptake of methane

Deleted: 4

The methane uptake over soil occurs over the unsaturated (upland) fraction of a grid cell that is not deemed wetland. The parameterization is based on an exact solution of the one-dimensional diffusion-reaction equation in the near-surface (top) soil layer and described in

Deleted: i.e. $(1-f_w)$

525 detail in Curry (2007). Briefly, the methane uptake by soil is a function of diffusion of
 526 methane into soil (which depends on atmospheric methane concentration) and its subsequent
 527 oxidation by microbes. The diffusion of methane into the soil depends primarily on air filled
 528 porosity of the soil and increases as the pore volume filled by liquid and frozen moisture
 529 decreases. The oxidation of methane by microbes is a function of both soil moisture and
 530 temperature. Oxidation preferably occurs when soils are neither too dry (when microbial
 531 activity is limited by low soil moisture) and nor too wet (when microbes are deprived of
 532 oxygen). Warmer temperatures favour oxidation of methane in soil and oxidation increases
 533 by about 4 times as soil temperature increases from 0 °C to 27.5 °C. Finally, the inhibition of
 534 methane uptake in cultivated soils is accounted for by a linear factor that reduces oxidation as
 535 crop fraction in a grid cell increases.

536 **2.1.2 Forcing data for the CLASS-CTEM model** 537

538 The CLASS-CTEM model is driven with meteorological data and atmospheric CO₂ and CH₄
 539 concentrations. The model also requires geophysical fields for the fractional coverage of nine
 540 CTEM PFTs, soil texture and depth to bedrock. The meteorological data are based on version
 541 7 of the Climate Research Unit – National Centre for Environmental Prediction (CRU-NCEP)
 542 reanalysis dataset (Viovy, 2012). The meteorological variables (surface temperature,
 543 pressure, precipitation, wind, specific humidity, and incident short-wave and long-wave
 544 radiation fluxes) are available at a spatial resolution of 0.5° × 0.5° and at a six hourly time
 545 interval for the period 1901-2015. These data are regridded to a spatial resolution of 2.81°
 546 and temporally to a half-hour time step to drive the CLASS-CTEM model. Temperature,
 547 pressure, wind, specific humidity, and long-wave radiation are linearly interpolated in time
 548 while short-wave radiation is assumed to change with the solar zenith angle with maximum
 549 radiation occurring at solar noon. Following Arora (1997) the six-hourly precipitation amount

550 (P , mm/6-hour) is used to estimate the number of wet half-hours in a given six-hour period
551 and the six- hourly precipitation amount is randomly distributed over these wet half hours.
552 Figure [B1 in Appendix B](#) shows the annual land-averaged temperature and precipitation
553 (excluding Antarctica) as derived from the CRU-NCEP data. Both temperature and
554 precipitation show an overall increase over the 20th century, that continues into the 21st
555 century, associated with the changing climate.

Deleted: 2

Deleted: ,

556
557 The land cover data are used by the model to specify the fractional coverage of CTEM's nine
558 PFTs in each grid cell. These data are based on a geographical reconstruction of the historical
559 land cover driven by the increase in crop area (Arora and Boer, 2010) but using the crop area
560 data based on the LUH2 v1h version of the Hurtt et al (2006) land cover product. The final
561 data set consists of the fractional coverage of CTEM's nine PFTs for the period 1850-2015 at
562 the global scale and at 2.81° spatial resolution. The increase in crop area over the historical
563 period leads to decrease in area of natural vegetation thus leading to deforestation. A fraction
564 of deforested vegetation is burned but deforested biomass is also converted to paper and
565 wood products which decompose over time leading to land use change emissions. These
566 processes are described in detail in Arora and Boer (2010). In context of terrestrial methane
567 budget, an increase in crop area leads to lower methane uptake by soil over the cultivated
568 fraction of a grid cell.

569
570 The globally averaged atmospheric CO₂ and CH₄ concentrations used to drive the model are
571 obtained from the data sets put together for the sixth phase of the Coupled Model
572 Intercomparison Project (CMIP6) and available from input4MIPs web site ([https://esgf-
573 node.llnl.gov/projects/input4mips/](https://esgf-node.llnl.gov/projects/input4mips/)). These data are shown in Figure [B2](#).

Deleted: 3

2.1.3 Observation and model-based data for CLASS-CTEM evaluation

In addition to evaluating the CLASS-CTEM simulated methane emissions from wetlands, fire and methane uptake by soils in the context of the one-box atmospheric CH₄ model as mentioned in section 2.2 below, we also evaluate simulated present-day wetland extent and all modelled methane fluxes directly against other model and observation-based estimates.

The CLASS-CTEM simulated wetland extent is compared against two data sets: the wetland data from the Global Lakes and Wetlands Database (GLWD; Lehner and Döll, 2004) and a new product that is formed by merging remote sensing based observations of daily surface inundation from the Surface Water Microwave Product Series (SWAMPS; Schroeder et al., 2015) with the static inventory of wetland area from the GLWD. The derivation of the second product is explained in detail in Poulter et al. (2017). SWAMPS provides estimates of fractional surface water based on data from multiple passive and active microwave satellite missions. While open water (e.g. rivers, lakes and ocean) and inundated wetlands comprising of open plant canopies are mapped by satellites, inundation beneath closed forest canopies, and exposed wetlands with water table below the surface cannot be mapped. However, satellite data are able to provide the seasonal cycle which static data sets like GLWD cannot. The merged SWAMPS-GLWD product attempts to overcome limitations of both individual data sets.

The simulated present-day methane emissions from wetlands and fire, and methane uptake by soil, are compared to top-down estimates compiled by Saunio et al. (2016). We also compare the anthropogenic emissions we have used within the framework of one-box atmospheric methane model (Section 2.2) with estimates from Saunio et al. (2016).

Field Code Changed

Field Code Changed

Field Code Changed

603 Finally, we also evaluate the model regionally over the West Siberian Lowlands (WSL). This
 604 region is chosen because inversion-based methane fluxes are readily accessible over the
 605 region which were compiled and documented for the WETCHIMP-WSL Intercomparison
 606 project (Bohn et al., 2015). We compare simulated wetland extent and wetland methane
 607 emissions with observation- and inversion-based results from Bousquet et al. (2011), Kim et
 608 al. (2011), and Winderlich (2012) and participating models in the Wetland and Wetland CH₄
 609 Intercomparison of Models Project (WETCHIMP, Melton et al. (2013)) focused on the West
 610 Siberian Lowlands region (WETCHIMP-WSL) (Bohn et al., 2015). Of these the Kim et al.
 611 (2011) and Winderlich (2012) are regional inversions. Kim et al. (2011) used wetland
 612 methane emissions from Glagolev et al. (2010) at 1° spatial resolution as their prior and used
 613 the NIES-TM atmospheric transport model for the period 2002–2007. They derived
 614 climatological monthly wetland emissions optimized to match atmospheric methane
 615 concentrations obtained by aircraft sampling. Winderlich (2012) used the Kaplan (2002)
 616 wetland inventory for prior wetland emissions with the TM3-STILT global inversion system
 617 for year 2009. Their posterior monthly wetland emissions were uniquely determined for each
 618 grid cell within their domain at 1° spatial resolution and optimized to match atmospheric
 619 methane concentrations measured at four tower observation sites located between 58°N and
 620 63 °N. The Bousquet et al. (2011) is a global inversion but uses two priors – the first one
 621 based on the Matthews and Fung (1987) emissions inventory and the second based on Kaplan
 622 (2002). Bousquet et al. (2011) inversion used the Laboratoire de Météorologie Dynamique
 623 general circulation model (LMDZ) atmospheric transport model at a 3.75° × 2.5° grid and
 624 estimated monthly methane emissions at a 1° spatial resolution for the period 1993–2009.
 625 Being a global inversion they optimized atmospheric concentrations relative to global surface
 626 observations at several flask stations for methane but also other trace gases. For wetland
 627 extent, we compare the CLASS-CTEM simulated wetland extent over the WSL region with

models participating in the WETCHIMP-WSL intercomparison, and GLWD and SWAMPS+GLWD products mentioned above but also the Global Inundation Extent from Multi-Satellites (GIEMS; Papa et al., 2010; Prigent et al., 2007) derived from visible and near-infrared and active and passive microwave sensors for the period 1993–2004. In addition, we also use the estimate from Peregon et al., (2009) who used a regional wetland typology map further refined by satellite image classifications to calculate the wetland extent in the WSL region.

2.2 Atmospheric methane – one box model, anthropogenic emissions and lifetime

2.2.1 One-box model of atmospheric methane

A one-box model of atmospheric CH₄ is used to evaluate the time evolution of simulated methane emissions from wetlands (E_w), methane emissions from fire (E_f) and the soil uptake of methane (S_{soil}) over the period 1850-2008. The model describes the changes in burden of atmospheric CH₄ (B) as a balance of surface emissions (consisting of natural, E_N , and anthropogenic emissions, E_A) and the atmospheric (S_{atmos}) and surface soil sinks (S_{soil}).

$$\frac{dB}{dt} = E_N(t) + E_A(t) - S_{atmos}(t) - S_{soil}(t) \quad (3)$$

where t is the time and equation (3) is applied at an annual time step. The atmospheric CH₄ burden (B , Tg CH₄) equals 2.78 times [CH₄] (represented in units of parts per billion, ppb) (Denman et al., 2007). The distinction between natural and anthropogenic emissions is not straight-forward for fire which contains emissions due to both natural and human-caused fires. For comparison with Saunois et al. (2016) global CH₄ budget (as shown later in Section 3) we consider all emissions from fire as anthropogenic, although the CLASS-CTEM model calculates fire emissions due both to lightning and human-caused ignitions. Natural emissions ($E_N = E_w + E_o$) consist of modelled wetlands emissions (E_w) and emissions from other

Deleted: 4

Deleted: 4

Field Code Changed

654 natural sources (E_o) (including termites, geological sources, wild animals and freshwater)
 655 which we specify at 25 Tg CH₄/yr (consistent with but towards the lower end of the range
 656 natural emissions, 21-130 Tg CH₄/yr, as deduced by top-down approaches summarized in
 657 Saunio et al. (2016)). The reason for specifying E_o at 25 Tg CH₄/yr is discussed later in
 658 section 4. Anthropogenic emissions ($E_A = E_{A \text{ excl fire}} + E_f$) consist of specified emissions
 659 from all anthropogenic sources excluding fire ($E_{A \text{ excl fire}}$) and fire emissions which we
 660 explicitly model (E_f). Estimation of anthropogenic emissions excluding those from fire and
 661 biomass burning ($E_{A \text{ excl fire}}$) data are explained in section 2.2.2.

Deleted: 30

Deleted: 0

Deleted: 30

Field Code Changed

662
 663 The atmospheric sink S is calculated as a first-order loss process from methane's lifetime
 664 τ_{chem} in the atmosphere as $S_{atmos}(t) = B(t)[1 - \exp(-1/\tau_{chem}(t))]$. An estimate of τ_{chem}
 665 is obtained from the Canadian Middle Atmosphere Model (CMAM) with chemistry and
 666 compared to an observation-based estimate from Prather et al. (2012) as later shown in
 667 Section 2.2.3. With S_{atmos} represented in terms of τ_{chem} equation (4) can be rewritten as

$$\begin{aligned} B(t + \Delta t) &= B(t) - B(t)[1 - \exp(-1/\tau_{chem}(t))] + (E_N(t) + E_A(t) - S_{soil}(t))\Delta t \\ &= B(t)[\exp(-1/\tau_{chem}(t))] + (E_N(t) + E_A(t) - S_{soil}(t))\Delta t \end{aligned} \quad (4)$$

Deleted: 5

670
 671 where $\Delta t = 1$ year. Equation (4) can be used to evaluate simulated natural methane emissions
 672 E_N in two ways. First, when all the terms on the right hand side of equation (4), including an
 673 initial value of $B(t)$, are known then the time evolution of B can be calculated and compared
 674 to its observation-based estimate. Second, if the time evolution of B is specified based on
 675 observations of methane concentration in the atmosphere then the value of τ_{chem} required to

Deleted: 5

Deleted: 5

satisfy equation (4) can be calculated (see equation 5) and compared its observation-based estimate e.g. from Prather et al. (2012).

Deleted: 5

Deleted: 6

$$\tau_{chem}(t) = - \frac{1}{\log\left(\frac{B(t+\Delta t) - (E_N(t) + E_A(t) - S_{soil}(t))\Delta t}{B(t)}\right)} \quad (5)$$

Deleted: 6

In section 3, we have used both these methodologies to assess CLASS-CTEM simulated methane emissions from wetlands (E_w), methane emissions from fire (E_f) and the soil uptake of methane (S_{soil}). Note that equation (4) does not include any term for oceanic methane emissions. Saunio et al. (2016) report a range of 0–5 Tg CH₄/yr, with a mean value of 2 Tg CH₄/yr for oceanic methane emissions. Given the large uncertainty in other components of the global methane budget, and the small magnitude of oceanic methane emissions, we have ignored this term.

Deleted: 5

Field Code Changed

Equation (3) may also be used to calculate pre-industrial methane concentration assuming atmospheric methane concentration was in equilibrium with pre-industrial emissions and sinks, i.e. by setting $\frac{dB}{dt} = 0$, which yields

$$E_N(t) + E_A(t) = S_{atmos}(t) + S_{soil}(t). \quad (6)$$

Substituting $S_{atmos}(t) = B(t)[1 - \exp(-1/\tau_{chem}(t))]$ similar to as was done in equation (4) and solving for $B(t)$ gives

$$B(t) = \frac{E_N(t) + E_A(t) - S_{soil}(t)}{1 - \exp(-1/\tau_{chem}(t))} \quad (7)$$

Deleted: exp

Using values of sources and sinks and τ_{chem} corresponding to year 1850, for example, yields $B(t)$ (Tg CH₄) which when divided by 2.78 yields [CH₄] in ppb for year 1850.

Formatted: Font: 12 pt

Formatted: Font: 12 pt

Formatted: Font: 12 pt

Formatted: Subscript

Formatted: Subscript

708 2.2.2 Anthropogenic methane emissions

709

710 The time evolution of global E_A (used in equation 4) for the 1850-2008 period is based on
711 two data sets. The first data set is the decadal representative concentration pathway (RCP)
712 anthropogenic methane emissions data set (version 2.0.5) available at 0.5° spatial resolution
713 for the period 1850-2000 and provided for the fifth phase of the coupled model
714 Intercomparison project (CMIP5) by the International Institute for Applied Systems Analysis
715 (IIASA) (<http://www.iiasa.ac.at/web-apps/tnt/RcpDb>). The value for the first year of each
716 decade is assumed to correspond to the rest of the decade. So the 1850 value corresponds to
717 the 1850-1859 decade, the 1860 value corresponds to the 1860-69 decade and so on. The
718 second anthropogenic methane emissions data set is part of version 4.2 of the Emission
719 Database for Global Atmospheric Research (EDGAR,
720 <http://edgar.jrc.ec.europa.eu/overview.php?v=42>) available at 0.1° spatial resolution and
721 available for the period 1970-2008. These data sets were selected because the RCP data set
722 provides the anthropogenic methane emissions going back to 1850 and the EDGAR data set
723 provides the anthropogenic methane emissions for more recent years since 1970. The
724 EDGAR data set was also chosen because amongst the recent anthropogenic data sets this is
725 the only data set which provides gridded anthropogenic methane emissions at an annual time
726 scale (see Table 1 of Saunio et al (2016)).

Deleted: 5

727

728 These two data sets are blended (or harmonized) to obtain a consistent time series of annual
729 global anthropogenic methane emissions for the period 1850-2008. First the RCP and
730 EDGAR data are regridded from their 0.5° and 0.1° spatial resolutions, respectively, to the
731 2.81° resolution at which the model is applied. Next all non-biomass burning emission
732 categories are added separately in both data sets to obtain total anthropogenic emissions for
733 each data set. The emissions categories in both data sets are somewhat different as shown in

Field Code Changed

Table 2. Emissions from fire and biomass burning are excluded because CLASS-CTEM simulates CH₄ emissions from fire explicitly. Since our framework requires only total anthropogenic methane emissions (excluding biomass burning) the different emissions categories in the two data sets do not matter. The wetland emissions from rice paddies, which we do not explicitly model, are included in the specified anthropogenic emissions (in category 11 of the EDGAR data set and category 1 of the RCP data set as shown in Table 2).

Equation (8) summarizes this harmonization methodology for a given grid cell.

$$E_{A,RCP \text{ adjusted}}(t) = E_{A,RCP}(t) + \frac{t-1850}{1970-1850} (E_{A,EDGAR}(1970) - E_{A,RCP}(1970)) \quad (8)$$

where $E_{A,RCP}$ and $E_{A,EDGAR}$ represent annual anthropogenic methane emissions (excluding biomass burning) in the RCP and EDGAR data sets, respectively, $E_{A,RCP \text{ adjusted}}$ represent the adjusted RCP emissions and t is the time in years from 1850 to 1970. The harmonization algorithm adjusts the annual total anthropogenic methane emissions in the RCP data, for each 2.81° grid cell, from 1850 to 1970 such that by the time RCP emissions reach 1970 they are the same as the EDGAR's total emissions excluding biomass burning. As a result of this harmonization, the largest change is made to RCP emissions for year 1970 and the smallest change is made for year 1851. The RCP emissions for year 1850 are not changed. The final harmonized time series for E_A is obtained by concatenating $E_{A,RCP \text{ adjusted}}$ for the period 1850 to 1970 and $E_{A,EDGAR}$ for the period from 1971 to 2008.

Figure 1a shows the harmonized time series of global anthropogenic methane emissions along with the decadal RCP and annual EDGAR emissions (excluding biomass burning). The RCP and EDGAR emissions are fairly similar for the period 1970-1990 but are different after 1990. Figures 1b and 1c illustrate how the harmonization works for two selected grid cells

765 based on equation (8). In Figure 1b anthropogenic methane emissions are shown for a land
 766 grid cell where emissions first increase and then decrease. In Figure 1c anthropogenic
 767 methane emissions are shown for an ocean grid cell, with six orders of magnitude lower
 768 emissions than the land grid cell, where emissions more or less continuously increase. In both
 769 case, the harmonization ensures that by 1970 the adjusted RCP emissions are same as the
 770 EDGAR emissions. Although for the purpose of using E_A in equation (4) only its global
 771 values are required, the methodology described here yields a continuous consistent gridded
 772 data set of anthropogenic methane emissions for the period of our analysis with no abrupt
 773 jumps.

Deleted: 7

Deleted: 4

Deleted: 4

Deleted: 5

774 775 **2.2.3 Lifetime of atmospheric methane** 776

777 To use equation (4), for evaluation of CLASS-CTEM simulated annual values of E_w , E_f and
 778 S_{soil} over the historical period, time-evolving annual values of τ_{chem} are required. We obtain
 779 values of τ_{chem} simulated by the Canadian Middle Atmosphere Model (CMAM). The
 780 CMAM is a fully interactive chemistry-climate model (CCM) that is based on a vertically
 781 extended version of the third generation Canadian Atmospheric General Circulation Model
 782 with a model lid at 95 km (Scinocca et al., 2008). The model contains a description of the
 783 important physical and chemical processes of the stratosphere/mesosphere and has been
 784 extensively assessed against observations through participation in two phases of the
 785 Chemistry-Climate Model Validation (CCMVal) activity (Eyring et al., 2006; SPARC
 786 CCMVal, 2010). Of more importance for methane, the chemistry has been extended
 787 throughout the troposphere by including cloud corrections on clear-sky photolysis rates,
 788 emissions of ozone precursors CO and NO_x (NO + NO₂) including emissions of NO_x from
 789 lightning, hydrolysis on specified tropospheric sulphate aerosols and interactive wet and dry

Deleted: 5

795 deposition. Note that the chemical mechanism currently used in CMAM has not yet been
796 extended to include the chemistry of non-methane hydrocarbons important in the
797 troposphere; only methane chemistry is considered.

798

799 Results from CMAM with tropospheric chemistry have been submitted to the Atmospheric
800 Chemistry and Climate Model Intercomparison Project (ACCMIP) (Lamarque et al., 2013).
801 The experimental design for ACCMIP involved timeslice simulations at various points in
802 time between 1850 and 2100, with simulations for year 2000 conditions used for assessing
803 the model chemical climate against available present-day observations. The ACCMIP
804 intercomparison found that the CMAM produced estimates of tropospheric chemical
805 quantities that fell well within the range of current generation CCMs. For example, the
806 present-day tropospheric ozone burden from CMAM was 323 Tg, versus a multi-model mean
807 of 337 ± 23 Tg, where the range is given as one standard deviation across the 15 participating
808 models (Young et al., 2013). The present-day methane lifetime to reaction with OH in the
809 troposphere was found to be 9.4 years, again well within the range of ACCMIP models of 9.7
810 ± 1.5 years (Naik et al., 2013). However, like the majority of ACCMIP models, the CMAM
811 predicts a too fast removal of CH₄ by OH as compared with our best-estimate from methyl-
812 chloroform decay of 11.2 ± 1.3 years (Prather et al., 2012). As described further below, the
813 calculated CH₄ lifetime to chemical loss from CMAM is therefore scaled to agree with
814 observationally-based estimates before being used in the one box atmospheric model of CH₄.

815

816 Time-dependent values of τ_{chem} are derived from a simulation over the 1850-2014 period
817 that uses specified sea-surface temperatures and sea-ice from one member of the five-member
818 historical ensemble performed by CanESM2 for the CMIP5. Data for 2006-2014 was taken
819 from a continuation of that simulation for the RCP 6.0 scenario. Specified anthropogenic and

Formatted: Subscript

biomass burning emissions of CO and NO_x were taken from the CMIP5 historical database (Lamarque et al., 2010) up to 2000 and for the RCP 6.0 scenario to 2014. Specified concentrations of long-lived greenhouse gases were from Meinshausen et al. (2011), following RCP 6.0 from 2006-2014. Specified stratospheric aerosol surface area density fields, used to account for the effects of large volcanic eruptions, was based on the 1960-2010 database created for the Chemistry Climate Model Initiative (CCMI) extended back to 1850 following the approach described in Neely III et al. (2016). Solar variability was included by calculating the wavelength-resolved daily variability relative to the long-term average (June 1976 – January 2007) from the recommended CMIP6 database (Matthes et al., 2017).

The observation-based estimate of τ_{chem} is obtained from Prather et al. (2012) who calculate

τ_{CH_4} based on equation (9) as

$$\frac{1}{\tau_{CH_4}} = \frac{1}{\tau_{OH}} + \frac{1}{\tau_{strat}} + \frac{1}{\tau_{trop-Cl}} + \frac{1}{\tau_{soil}} = \frac{1}{\tau_{chem}} + \frac{1}{\tau_{soil}} \quad (9)$$

where τ_{OH} (present day value of 11.2 years), τ_{strat} (120 years), $\tau_{trop-Cl}$ (200 years) and τ_{soil} (150 years) are the lifetimes associated with the destruction of CH₄ by tropospheric OH radicals, loss in the stratosphere, reaction with tropospheric chlorine and uptake by soils, respectively, which yields a present day (corresponding to year 2010) value of τ_{CH_4} as 9.1±0.9 years. τ_{chem} is the methane life time associated with chemical processes in the atmosphere. For the pre-industrial period (corresponding to year 1750), Prather et al. (2012) estimate τ_{CH_4} as 9.5±1.3 years assuming τ_{OH} to be equal to 11.76 years (based on Atmospheric Chemistry and Climate Model Intercomparison Project (ACCMIP) results (Voulgarakis et al., 2013)) and lifetimes associated with other processes are assumed to stay the same. In our study, the methane soil sink is explicitly simulated in the CLASS-CTEM

Deleted: 8

Deleted: 8

845 framework and this corresponds to the term $\frac{1}{\tau_{soil}}$ in equation (9). The remaining terms in
846 equation (9) all correspond to atmospheric processes. Removing the $\frac{1}{\tau_{soil}}$ term in equation (9)
847 gives us an observation-based estimate of τ_{chem} making it consistent with CMAM's methane
848 lifetime corresponding only to atmospheric processes and increases the observation-based
849 estimates of pre-industrial and present-day atmospheric CH₄ lifetimes to 10.15±1.45 years
850 and 9.7±1.0 years, respectively.

Deleted: 8

Deleted: 8

Deleted: 8

851
852 Figure 2 compares the τ_{chem} values from CMAM with its observation-based estimate from
853 Prather et al. (2012) and shows that CMAM based estimates are biased low and outside the
854 uncertainty range of observation-based estimates, as mentioned earlier. When used in the
855 one-box model of atmospheric methane, the lower than observed τ_{chem} values will
856 inevitably lead to a higher than observed atmospheric sink (S_{atmos}) and thus lower than
857 observed atmospheric methane concentration even if all the other flux terms (E_N , E_A , and
858 S_{soil}) in equation (5) are realistic. We therefore adjust the CMAM derived values of τ_{chem}
859 upwards by 15% so that they lie within the uncertainty range of observation-based estimates
860 of the τ_{chem} as derived by Prather et al. (2012). These adjusted values of τ_{chem} are also
861 shown in Figure 2.

Deleted: 5

Deleted: 5

863 2.3 The experimental setup

864

865 2.3.1 Equilibrium pre-industrial simulation

866

867 The equilibrium pre-industrial simulation was initialized from zero biomass for all PFTs. The
868 fractional coverages of CTEM's nine PFTs for the pre-industrial simulation are based on the

land cover product described in section 2.1.2 for year 1850. The model was then driven with 1901-1925 CRU-NCEP climate data cycled repeatedly until the model pools reach equilibrium. The early part of the 20th century does not show any significant trends compared to the later part of the 20th century, as seen in Figure [B1 \(Appendix B\)](#), so using the 1901-1925 data to spin up the model to equilibrium for 1850 conditions is reasonable. Atmospheric CO₂ and CH₄ concentration levels were set to 285 ppm and 791 ppb, respectively, corresponding to their pre-industrial 1850 levels. This pre-industrial equilibrium simulation yields initial conditions for all CLASS-CTEM prognostic variables for the transient 1851-2015 simulation.

Deleted: 2a

2.3.2 Transient historical simulation

The transient historical simulation is performed for the period 1851-2015 and its prognostic variables are initialized from the equilibrium pre-industrial simulation as mentioned above. For the period 1851 to 1900 of this simulation the model is driven with meteorological data from 1901-1925 twice similar to what [was done for](#) spinning up the model for the pre-industrial simulation. For the period 1901-2015 the meteorological data corresponding to each year are used. Time varying concentrations of atmospheric CO₂ and CH₄ are specified for the period 1851-2015. The annual time-varying fractional coverages of C₃ and C₄ crop PFTs in each grid cell are based on LUH2 v1h version of the Hurtt et al (2006) land cover product.

Deleted: we do for

In this transient simulation, 1) wetland extent and its methane emissions respond to changes in climate but also increases in atmospheric CO₂ concentration (which increases net primary productivity and thus heterotrophic respiration), 2) methane emissions from fire respond to

901 changes in climate, atmospheric CO₂ concentration, population density and land use change,
902 and 3) methane uptake by soil responds to climate, changes in atmospheric CH₄ concentration
903 and changes in crop fraction.

904

905 3. Results

906

907 We first show the results from the transient 1851-2015 simulation and evaluate the time-
908 evolution of CLASS-CTEM simulated global natural methane fluxes over the historical
909 period using the one-box model of atmospheric methane described in section 2.2. This is
910 followed by evaluation of model fluxes for the present day against observation-based
911 estimates and for the WSL region using observation-based estimates and results from other
912 models.

913

914 3.1 Time evolution of simulated global natural methane fluxes

915

916 Figure 3 shows the time evolution of simulated annual maximum wetland extent, methane
917 emissions from wetlands and fire, and soil uptake by methane from the 1851-2015 transient
918 historical simulation. In Figure 3: 1) the simulated wetland methane emissions increase by
919 30% over the historical period from about 130 to 169 Tg CH₄/yr from 1850s to the present
920 day (2000-2008) partly due to increase in wetland extent which increases by 8% from 7.5 to
921 8.1 million km² from 1850s to the present day, 2) the simulated fire methane emissions
922 decrease from their 1850s value by 20% from about 34 to 27 Tg CH₄/yr for the present day
923 and 3) the soil methane uptake more than doubles from its 1850s value of about 14 to 29 Tg
924 CH₄/yr for the present day.

Deleted: 6

Deleted: 6

927

928 The increase in wetland methane emissions over the historical period is due to an increase in
929 the wetland area, driven by increase in precipitation seen in Figure [B1 \(Appendix B\)](#), but also
930 higher methane fluxes per unit area. The higher methane fluxes per unit area are caused by
931 increase in atmospheric CO₂ concentration which increases both net primary productivity and
932 heterotrophic respiration over the historical period as shown in Figure [C1 in Appendix C](#).
933 Since wetland methane emissions are proportional to heterotrophic respiration (R_h) in
934 equation (2) an increase in R_h also increases methane emissions from wetlands.

Deleted: 2b

Deleted: 7

Deleted: 3

935

936 The decrease in methane emissions from wildfires is driven by a decrease in area burned
937 which itself is driven by an increase in crop area and population density over the historical
938 period ([Arora and Melton, 2018](#)). The increase in cropland area decreases area burned by
939 wildfires in the model since croplands are not allowed to burn. In the real world cropland area
940 also fragments the landscape which affects the spread of fire. Direct anthropogenic influences
941 on wildfires are more complex since accidental, as well as intentional, human-caused
942 ignitions enhance wildfires while anthropogenic suppression of wildfires decreases area
943 burned and fire related emissions. Figure [C2 \(Appendix C\)](#) shows that the overall effect of
944 increase in crop area and population density in the model is that area burned increases
945 slightly up to about 1930, and then starts decreasing thereafter and this area burned pattern
946 compares reasonably with the decadal charcoal index from the Global Charcoal Database
947 version 3 (Marlon et al., 2008) for the full length of the historical simulation. Winds and
948 smoke carry charcoal from fires and deposit it onto aquatic sediments and this forms the basis
949 of sediment charcoal indices. The caveat with the comparison with sediment charcoal records
950 is that they provide only a proxy for fire activity and indicate if fire activity is higher or lower
951 relative to a point in time. Figure [C2](#) also compares area burned with estimates from version

Formatted: Font: (Default) Times New Roman, 12 pt

Deleted: ¶

Deleted: 8

Deleted: 2

Deleted: 8

4.1s of the Global Fire Emissions Database (Giglio et al., 2013; Randerson et al., 2012) that are based on the satellite record and available only for the short 1997-2014 period. Model and observation-based average burned area over this 1997-2014 period are 483.4 and 485.5 million hectares year⁻¹ and their trends are -5.57 ± 1.25 and -3.43 ± 1.05 million hectares year⁻², respectively. The negative trends indicate burned area has been decreasing.

Finally, the increase in methane uptake by soils is primarily the response to an increase in the atmospheric concentration of methane. Diffusion of methane into the soil is directly proportional to its atmospheric concentration (Curry, 2007) which more than doubles from around 790 ppb in 1850 to around 1830 ppb in 2015 (Figure B2, panel b).

Deleted: 3b

3.2 Evaluation of simulated global natural methane fluxes

We first evaluate the CLASS-CTEM simulated global natural methane fluxes in a forward simulation where all the right hand side terms of equations (3) and (4) are specified at an annual time step and the change in atmospheric methane burden $\frac{dB}{dt}$ is calculated every year.

Deleted: 5

Although the CRU-NCEP meteorological data are available to 2015 allowing us to perform offline CLASS-CTEM simulations up until 2015, the last year for which harmonized RCP-EDGAR emissions are available is 2008. We therefore simulate the time evolution of atmospheric methane concentration for the period 1851-2008. In this forward calculation of atmospheric methane burden the one box model may be initialized using the observed 1850 methane concentration or using the 1850 concentration that is in equilibrium with 1850 sinks

and sources. The latter is calculated by assuming $\frac{dB}{dt} = 0$ as illustrated in equations (6) and (7). The numerator term in equation (7) ($E_N(t) + E_A(t) - S_{soil}(t)$) for year 1850 is 214.2 Tg

Deleted: in equation (5) and finding the value of B for all other terms correspond to their 1850 values

Formatted: Font: 12 pt

Formatted: Font: 12 pt

Formatted: Font: 12 pt

Formatted: Font: 12 pt

Formatted: Font: 12 pt

Formatted: Font: 12 pt

Formatted: Font: 12 pt

Formatted: Font: 12 pt

Formatted: Font: 12 pt

Formatted: Font: 12 pt

Formatted: Font: 12 pt

Formatted: Font: 12 pt

CH₄/year (wetland emissions are 130.1, other natural emissions are specified at 25, anthropogenic emissions are 39.5, fire emissions are 33.2, and soil uptake is 13.6). In equation (7) using adjusted CMAM τ_{chem} value of 8.82 years (for year 1850, red line in Figure 2) yields an 1850 equilibrium [CH₄] for 1850 of 719 ppb compared to its observation-based value of 791 ppb. In contrast, using the midrange value of τ_{chem} of 9.97 years based on Prather et al. (2012) yields equilibrium [CH₄] for 1850 of 808 ppm which compares much better with its observation-based estimate of 791 ppm. An equilibrium methane concentration in 1850 that is lower than observed, when using adjusted CMAM τ_{chem} , implies that the atmospheric methane sink is higher and associated with lower than observed atmospheric methane lifetime in 1850. Indeed, the adjusted CMAM τ_{chem} for 1850 of 8.82 years is less than Prather et al. (2012) midrange estimate of 9.97 years but still within their uncertainty range as seen in Figure 2. Regardless, since the lifetime of methane in the atmosphere is only around 10 years the effect of initial conditions disappears by around 1870. This is shown in Figure 4a which compares the simulated evolution of atmospheric methane burden with its observations using the adjusted CMAM τ_{chem} . Figure 4a shows that overall the simulated increase in methane concentration over the historical period is reasonable compared to observation-based estimates despite the various specified and modelled sources and sinks that contribute to the time evolution of atmospheric methane burden. In Figure 9a, the coefficient of correlation between observation-based (black line) and simulated (green and blue lines) [CH₄] is 0.99 and root mean square error (RMSE) is 35 ppb (green line) and 41 ppb (blue dashed line). The simulated values are somewhat overestimated from 1885 to 1980 and underestimated from 1980 to 2005. The increase in observed methane concentration over the 1850 to 2008 period is 998 ppb, while the one box model yields an increase of 1006 ppb when initialized from observed 1850 methane concentration. The year 2008 concentration is calculated to be 1797 ppb compared to the observation-based value of 1790 ppb.

Formatted: Subscript

Formatted: Font: 12 pt

Formatted: Font: 12 pt

Formatted: Font: 12 pt

Deleted: in 1850

Deleted: 708

Formatted: Font: 12 pt

Deleted: . This yields an

Deleted: concentration

Formatted: Font: (Default) Times New Roman, 12 pt

Formatted: Font: (Default) Times New Roman, 12 pt

Formatted: Subscript

Deleted: the 1850 emissions are lower and/or

Deleted: (

Deleted:)

Deleted: .

Deleted: 9

Deleted: 9

Formatted: Subscript

Deleted: 1024

Deleted: 1815

1027

1028 An alternative approach to evaluate the modelled natural sinks and sources is to specify the
1029 rate of increase of atmospheric methane burden according to its observations and calculate
1030 the required atmospheric lifetime of methane (excluding the soil sink), given modelled
1031 natural sinks and sources, following equation (5) as discussed in section 2.2. These results are
1032 shown in Figure 4b, which compares the methane lifetimes required to achieve the observed
1033 increase in methane concentration over the historical period (black line) to within ± 3 ppb
1034 (shaded area between grey lines) with observation-based estimate of atmospheric methane
1035 lifetime based on Prather et al. (2012) and the adjusted atmospheric methane lifetime from
1036 CMAM (both of which were shown earlier in Figure 2). Figure 4b shows that for the most
1037 part, the calculated atmospheric methane lifetime stays within the uncertainty of observation-
1038 based estimates. More over the temporal trend after 1900 in calculated atmospheric methane
1039 lifetime compares well to the trend in the atmospheric methane lifetime from the CMAM
1040 model. Both anthropogenic emissions and methane concentration during the early part of the
1041 1850-2008 historical period are more uncertain than during the later part and therefore the
1042 differences between simulated and observation-based estimates of atmospheric methane
1043 concentration (in Figure 4a) and methane lifetimes (in Figure 4b) for the period 1850-1900
1044 are not unexpected.

1045

1046 While the results in Figures 4a and 4b provide some confidence that the magnitude and
1047 temporal evolution of simulated global natural methane sources and sinks over the historical
1048 period are reasonable they, of course, do not allow the evaluation of all of the simulated
1049 natural fluxes individually.

1050

Deleted: 6

Deleted: 9

Deleted: 5

Deleted: 5

Deleted: 9

Deleted: 9

Deleted: 9

Deleted: 9

Deleted: 9

1060 We also evaluate the role of increase in wetland methane emissions over the historical period
 1061 (as seen in Figure 3) on the historical methane budget. Instead of using wetland methane
 1062 emissions from the transient historical simulation in the one box model of atmospheric
 1063 methane we use wetland methane emissions from the equilibrium pre-industrial simulation in
 1064 which 1901-1925 CRU-NCEP meteorological data are used repeatedly and CO₂ is held
 1065 constant at its pre-industrial level of 285 ppm. As a result wetland extent and methane
 1066 emissions do not respond to changes in climate and increasing CO₂, and do not increase over
 1067 the historical period (as seen in Figure 5a). Methane emissions from fire and soil uptake of
 1068 methane still respond to changes in climate and increasing CO₂. The result of using these
 1069 wetland methane emissions (shown in Figure 5a) in the framework of the one box model of
 1070 atmospheric methane is shown in Figure 5b. In Figure 5b, although [CH₄] overall increases
 1071 over the historical period in response to increase in anthropogenic emissions, the result of
 1072 wetland methane emissions not increasing over the historical period is that the simulated
 1073 atmospheric methane concentration in year 2008 is calculated to be 1667 ppm, which is 130
 1074 ppb lower than the 1797 ppb seen in Figure 4a.

Deleted: 6

Deleted: 10

Deleted: 10

Deleted: 10

Deleted: 10

Deleted: 1685

Deleted: 1815

Deleted: 9

1075 1076 3.3 Geographical distribution of wetland extent

1077
 1078 Figure 6 compares the zonally-averaged maximum wetland fraction over land with
 1079 observation-based estimates based on the Global Lakes and Wetland (GLWD; Lehner and
 1080 Döll, 2004) and the new product formed by merging remote sensing based observations of
 1081 daily surface inundation from the Surface Water Microwave Product Series (SWAMPS;
 1082 Schroeder et al., 2015) with the static inventory of wetland area from the GLWD from
 1083 Poulter et al. (2017), as mentioned earlier in section 2.1.3. Maximum wetland fraction from
 1084 the model and SWAMPS+GLWD product is calculated as the maximum of 12 mean monthly

Deleted: 11

Field Code Changed

1094 | values from the 13 years spanning the 2000-2012 period. Figure 6 shows that overall the
1095 | model is able to capture the broad latitudinal distribution of wetlands with higher wetland
1096 | fraction at northern high-latitudes and in the tropics. The model yields higher wetland
1097 | fraction in the tropics than both observation-based estimates and this is due to higher wetland
1098 | fraction simulated in the Amazonian region. The Amazonian region is densely forested and
1099 | the SWAMPS product is unable to map wetlands beneath closed forest canopies. Biases also
1100 | likely exist in the GLWD data set since parts of the Amazonian region are fairly remote. This
1101 | is shown in Figure 7 which compares the geographical distribution of simulated maximum
1102 | wetland fraction with that from the GLWD and SWAMPS+GLWD products. The model
1103 | successfully captures wetlands in the Hudson Bay lowlands, the West Siberian lowlands, the
1104 | Pantanal and the region bordering Argentina, Paraguay and Uruguay in South America,
1105 | Indonesia and the low lying region around Bangladesh. In terms of differences from these
1106 | observation-based data sets the model most notably overestimates wetland extent in Europe.
1107 | One possible reason for this is that wetlands in Europe have been drained for agriculture and
1108 | our wetland parameterization does not take this into account. About two-thirds of the
1109 | European wetlands that existed 100 years ago have been lost (European Commission, 1995)
1110 | leading to a substantial decrease in the number and size of large bogs and marshes, and small
1111 | or shallow lakes.

Deleted: 11

Deleted: 12

1113 3.4 Geographical distribution of simulated natural fluxes

1114
1115 | Figure 8 shows the geographical distribution of methane emissions from dynamic wetlands
1116 | (panel a) and fire (panel b) and the soil uptake of methane (panel c) simulated by the CLASS-
1117 | CTEM model. The figures also show the global total of these fluxes averaged over the 2000-
1118 | 2008 period for later comparison with estimates from Saunio et al. (2016). Methane

Deleted: 13

Field Code Changed

emissions from wetlands (168.9 Tg CH₄/yr) are the largest of natural fluxes, as is well known, while emissions from fire (26.8 Tg CH₄/yr) and methane uptake by soil (28.7 Tg CH₄/yr) are an order of magnitude lower. As expected, the geographical distribution of methane emissions from wetlands (Figure 8a) corresponds well to the geographical distribution of wetlands themselves (Figure 8a) although per unit wetland area methane emissions are higher in tropics and milder temperate regions than in high-latitude regions. This is because warmer temperatures and longer growing season in the tropical and milder temperate regions imply that wetlands can emit more methane per unit wetland area and for a longer period of time than the colder high-latitude regions with a shorter growing season. In Figure 8b the geographical distribution of methane fire emissions shows higher values in seasonally-dry tropical regions and order of magnitudes lower values in mid-high latitude regions. These results are consistent with area burned (not shown) which shows a similar pattern (Arora and Melton, 2018). Finally, the geographical distribution of methane uptake by soils in Figure 8c shows higher methane uptake by soils in parts of arid regions (including the Sahara and the Australian outback) where soil moisture doesn't get too dry (so as to not excessively limit soil microbial activity) but otherwise fairly uniform uptake in the tropics and lower values in mid-high latitude regions where lower temperatures and higher soil moisture limit methane uptake by soils.

Deleted: 13

Deleted: 12

Deleted: 13

Formatted: Font: (Default) Times New Roman, 12 pt

Deleted: 13

Deleted: dry

3.5 Regional evaluation over West Siberia lowlands

While evaluation of simulated global wetland extent and wetland methane emissions, and their geographical distribution, provides confidence in model results, we further evaluate the model at a regional scale over the West Siberia lowlands. The model results are sampled for the region lying between 50 to 75 °N and 60 to 95°E for comparison with observation- and inversion-based estimates (mentioned earlier in section 2.1.3). Figure 9a compares CLASS-

Deleted: 14

CTEM simulated wetland extent with those from models participating in the WETCHIMP-WSL intercomparison, and the GIEMS, SWAMPS and merged SWAMPS and GLWD products mentioned in section 2.1.3. Table 2 compares the simulated annual maximum wetland extent with models participating in the WETCHIMP-WSL intercomparison and these observation-based products. All values are reported as average for the period 1993-2004 except for the merged SWAMPS and GLWD product whose average is for the 2002-2012 period, and the Peregon et al. (2009) estimate that is based on wetland typology map from a 1977 publication and a more recent satellite land cover product. CLASS-CTEM simulated monthly wetland extent in Figure 9a compares best with the merged SWAMPS and GLWD product, while both the satellite-based inundation products by themselves (SWAMPS and GIEMS) show much lower values. Satellite-based products that remotely sense inundated areas can only do so when water table is above the ground and therefore wetland areas inferred from these products are expected to be lower in magnitude than products which also take into account land cover as is the case for the merged SWAMPS and GLWD product.

Deleted: 3

Deleted: 14

In Table 2, the annual maximum wetland extent is quite similar for the merged SWAMPS and GLWD product (0.55 million km²) and CLASS-CTEM simulated values (0.53 million km²) but the maximum occurs in different months. In Figure 9b, for the merged SWAMPS and GLWD product the maximum wetland extent occurs in June while CLASS-CTEM simulated values show peak both in June and September. The participating models from the WETCHIMP-WSL intercomparison show a range of values for the monthly wetland extent in the WSL region (Figure 9a). Models range from those which specify constant values with no seasonality for the wetland extent to models which dynamically model wetland extent two of which show maximum wetland extent of greater than 1 million km². The average annual maximum wetland extent across the participating models in the WETCHIMP-WSL is

Deleted: 3

Deleted: 14

Deleted: 14

1184 0.70±0.15 million km² (mean ± standard error). Finally, the Peregon et al. (2009) estimate is
1185 0.68 million km² which is somewhat higher than the CLASS-CTEM simulated value (0.53
1186 million km²) and the merged SWAMPS and GLWD product (0.55 million km²).

1187

1188 Figure 9b compares CLASS-CTEM simulated monthly wetland methane emissions with
1189 those from models participating in the WETCHIMP-WSL intercomparison and four
1190 inversion-based estimates mentioned in section 2.1.3. The two Bousquet et al. (2011)
1191 inversions shown in Figure 9b correspond to ones using the reference Matthews and Fung
1192 (1987) emissions inventory (Bousquet 2001 R) and the emissions inventory based on Kaplan
1193 (2002) (Bousquet 2001 K). All values are reported as average for the period 1993-2004
1194 except for the Kim et al. (2011) inversion which reports fluxes for year 2005 and the
1195 Winderlich (2012) inversion which corresponds to year 2009.

1196

1197 Table 2 compares the simulated annual wetland methane emissions from CLASS-CTEM with
1198 those from models participating in the WETCHIMP-WSL intercomparison and the four
1199 inversion-based estimates. In Table 2, the inversion-based annual wetland methane emissions
1200 vary from 3.08 to 9.80 Tg CH₄/yr. The highest annual emissions in the Winderlich (2012)
1201 inversion are due to higher emissions in the shoulder months of spring and fall compared to
1202 other inversions but also non-zero emissions during winter months (December to February)
1203 as seen in Figure 9b. The CLASS-CTEM model calculates annual wetland methane
1204 emissions of 7.76 Tg CH₄/yr and the average for models participating in the WETCHIMP-
1205 WSL intercomparison is 5.34±0.54 Tg CH₄/yr (mean ± standard error). Of all the models and
1206 inversions only the Winderlich (2012) inversion shows substantial methane emissions for the
1207 November to April period. In CLASS-CTEM as the liquid soil moisture in the top soil layer
1208 freezes wetland extent contracts to zero (Figure 9a) and methane emissions are shut off

Deleted: 14

Deleted: 14

Deleted: 3

Deleted: _

Deleted: 3

Deleted: 14

Deleted: 14

1216 during the winter months. Bohn et al. (2015) note that Winderlich (2012) inversion-based
1217 estimates may have been influenced by emissions from fossil fuel extraction and biomass
1218 burning, although the seasonality of Winderlich (2012) fluxes, with non-zero emissions even
1219 in winter, is plausible. Based on year-round eddy flux measurements of methane emissions
1220 from an Alaskan Arctic tundra sites Zona et al. (2016) find that cold season (September to
1221 May) emissions account for $\geq 50\%$ of the annual methane flux, with the highest emissions
1222 from non-inundated upland tundra. They find a major fraction of cold season emissions occur
1223 during the “zero curtain” period, when subsurface soil temperatures are near 0 °C. Langer et
1224 al., (2015) report winter emissions from tundra ponds in Siberia as they are freezing during
1225 early winter. They analyzed concentrations of methane in bubbles (trapped in the lake ice)
1226 which were higher at depths than at the ice surface. So it is entirely plausible that methane
1227 emissions occur during transition to winter months which models fail to simulate and most
1228 inversions fail to capture.

Moved down [1]: So it is entirely plausible that methane emissions occur during winter months which models fail to simulate and most inversions fail to capture.

Formatted: Font: (Default) Times New Roman, 12 pt

Formatted: Font: (Default) Times New Roman, 12 pt

Moved (insertion) [1]

1230 3.6 Evaluation of present-day global methane budget

1231
1232 Our final evaluation of simulated global methane budget is against estimates compiled by
1233 Saunois et al. (2016) who synthesize several recent studies to summarize the present-day
1234 global methane budget. Our global methane budget is based on simulated and specified fluxes
1235 and the use of one box model of atmospheric methane. We exclusively evaluate our
1236 simulated global methane budget against the top-down approaches presented in Saunois et al.
1237 (2016) since estimates from bottom-up approaches are known to yield higher total emissions
1238 than those based on top-down approaches as mentioned earlier in the Introduction. The global
1239 methane budget based on top-down approaches which are constrained by the atmospheric
1240 CH₄ burden and its loss in the atmosphere is considered more reliable than that based on the

Field Code Changed

Field Code Changed

1245 bottom-up approaches. These comparisons are shown in Table 3. The natural and
 1246 anthropogenic sources are divided into their broad categories and so are the sinks which are
 1247 divided into atmospheric and soil sinks. The Saunois et al. (2016) estimates are reported for
 1248 the period 2000-2009 while the CLASS-CTEM values correspond to the 2000-2008 period
 1249 since the EDGAR anthropogenic emissions were available only until 2008 at the time of this
 1250 study and therefore the one box model of atmospheric methane is also run up until 2008. For
 1251 clarity, Table 3 also identifies which fluxes are modelled by CLASS-CTEM, which are
 1252 specified and which are based on atmospheric methane lifetimes.

Deleted: 4

Field Code Changed

Deleted: 4

1253
 1254 In Table 3 the total emissions from natural sources in our framework are 199 Tg CH₄/yr
 1255 which are in the lower part of the range of 194-292 Tg CH₄/yr compiled by Saunois et al.
 1256 (2016). This is due to lower specified emissions from non-wetland sources. While our
 1257 modelled emissions from wetlands of 169 Tg CH₄/yr compare well with the Saunois et al.
 1258 (2016) central estimate of 166 Tg CH₄/yr, our specified emissions from other natural sources
 1259 (including termites, geological sources and fresh water bodies) of 25 Tg CH₄/yr are near the
 1260 low end of their range (21-130 Tg CH₄/yr). In contrast, our anthropogenic emissions of 344
 1261 Tg CH₄/yr (which include emissions from fire for consistency with Saunois et al. (2016)) are
 1262 higher than Saunois et al. (2016) central estimate of 319 Tg CH₄/yr and towards the higher
 1263 end of their range (255-357 Tg CH₄/yr). This is due to the use of EDGAR emissions which as
 1264 Saunois et al. (2016) note are towards the higher end of all data sets of anthropogenic
 1265 emissions. Our modelled fire emissions of 27 Tg CH₄/yr are lower than Saunois et al. (2016)
 1266 central estimate of 35 Tg CH₄/yr. One reason for this is that while we include natural and
 1267 anthropogenic fires in our framework we do not account for biofuel burning. Overall, our
 1268 emissions from natural sources are 35 Tg CH₄/yr lower, and emissions from anthropogenic
 1269 sources are 25 Tg CH₄/yr higher, than the Saunois et al. (2016) central estimates. As a result,

Deleted: 4

Field Code Changed

Field Code Changed

Deleted: 30

Field Code Changed

Field Code Changed

Field Code Changed

Field Code Changed

Field Code Changed

1274 the sum of natural and anthropogenic emissions (543 Tg CH₄/yr) in our framework is 9 Tg
1275 CH₄/yr lower than Saunois et al. (2016) central estimate (552 Tg CH₄/yr).

Field Code Changed

1276
1277 The total sink strength is calculated to be 538 Tg CH₄/yr in our framework which compares
1278 well with the Saunois et al. (2016) estimate of 546 Tg CH₄/yr. Saunois et al. (2016) do not
1279 provide uncertainty ranges for the atmospheric and total sink. The modelled atmospheric (509
1280 Tg CH₄/yr) and soil (29 Tg CH₄/yr) sinks in Table 3 also compare well with Saunois et al.
1281 (2016) estimates of 514 and 32 Tg CH₄/yr, respectively.

Field Code Changed

Field Code Changed

Deleted: 4

Field Code Changed

1283 4. Discussion and conclusions

1284
1285 The offline evaluation of natural methane fluxes simulated by the CLASS-CTEM modelling
1286 framework presented here is the first step in making atmospheric methane concentration a
1287 prognostic variable in the family of Canadian earth system models. The evaluation is based
1288 on comparison of present-day fluxes with existing observation- and model-based estimates
1289 compiled by Saunois et al. (2016) but also the historical evolution of atmospheric methane
1290 burden and methane's lifetime simulated using a one box model of atmospheric methane.
1291 While our simulated and specified present-day global methane budget components lie within
1292 the uncertainty range for top-down estimates from Saunois et al. (2016) this also implies that
1293 methane emissions from individual sectors for the present-day budget can be increased or
1294 decreased within their uncertainty ranges as long as the total emissions stay the same. The
1295 time evolution of the atmospheric methane burden over the historical period, however,
1296 provides additional constraints than the present-day methane budget. For example, our
1297 specified methane emissions of 25 Tg CH₄/yr from other nature sources (E_o) (including
1298 termites, geological sources, wild animals and freshwater) are lower than Saunois et al.

Field Code Changed

Deleted: uncertainty range

Field Code Changed

Deleted: 30

Field Code Changed

1302 (2016) central estimate of 68 Tg CH₄/yr, although still within their uncertainty range (21-130
 1303 Tg CH₄/yr). In the absence of any information about its time evolution we have assumed that
 1304 E_o remains constant over the historical period. This is a plausible assumption since we do not
 1305 expect emissions from termites, geological sources, wild animals and freshwater to show a
 1306 large response to changing environmental conditions over the historical period. Certainly, not
 1307 as large as we saw for wetland emissions which increased by 40 Tg CH₄/yr over the 1850-
 1308 2008 period (Figure 3). However, when we use a constant E_o of 68 Tg CH₄/yr in our
 1309 framework we obtain higher than observed methane concentration throughout the historical
 1310 period and the year 2008 value is 1953 ppb compared to 1797 ppb that we obtain in Figure 4a
 1311 (observed methane concentration for 2008 is 1790 ppb). This is shown in Figure 10. Part of
 1312 the reason for this may be that present-day EDGAR emissions are higher than other estimates
 1313 as Saunio et al. (2016) note and that's why we had to choose a lower E_o . However, the
 1314 global harmonized and RCP anthropogenic emissions are fairly similar up until 1990 (see
 1315 Figure 1a) and therefore had we use RCP based emissions (up until year 2000) we still would
 1316 have obtained higher than observed atmospheric methane concentrations throughout the
 1317 historical period when using E_o of 68 Tg CH₄/yr. Our framework cannot accommodate E_o
 1318 larger than about 25-30 Tg CH₄/yr without overestimating atmospheric methane
 1319 concentrations throughout the historical period.

Deleted: 6

Deleted: 1815

Deleted: 9

Deleted: 5

Field Code Changed

Deleted: 4

Deleted: 3

Deleted: 0

Deleted: 35

Deleted:

Deleted: 10

1321 The second constraint provided by the time evolution of the atmospheric methane burden
 1322 over the historical period is that related to wetland methane emissions. As seen in section 3.2,
 1323 in the absence of the simulated increase in wetland methane emissions from about 130 to 170
 1324 Tg CH₄/yr from 1850s to the present day the simulated year 2008 atmospheric methane
 1325 concentration is about 100 ppb lower than observed (as seen in Figure 5). Assuming our RCP
 1326 and EDGAR based harmonized anthropogenic emissions and their increase over the historical

1337 period is reasonably realistic, this indicates that it is very likely that wetland methane
1338 emissions have indeed increased over the historical period in response to changes in climate
1339 and increased atmospheric CO₂ concentration. The results in section 3.1 showed that this
1340 increase of 30% in wetland methane emissions is driven more by an increase in methane
1341 emissions per unit area than the increase in maximum wetland extent, which increased by
1342 about 8% over the historical period. The implication of this is that wetland methane
1343 emissions will likely keep increasing in the future in response to the increasing atmospheric
1344 concentration of CO₂ driven by higher heterotrophic respiration.

1345

1346 The evaluation of simulated wetland extent against the GLWD and the merged SWAMPS
1347 and GLWD product provides confidence that the model is broadly able to reproduce the
1348 geographical distribution of wetlands although, of course, some limitations remain. Over the
1349 WSL region the simulated estimates of wetland extent and wetland methane emissions are
1350 also broadly consistent with observation-based estimates.

1351

1352 The version of the model used here treats its land mask as binary so each grid cell is either
1353 land or ocean/water. While the model is capable of representing inland lakes using a separate
1354 tile (and simulate the resulting impact on energy and water fluxes) this functionality was not
1355 used in this study. In addition, representation of inland lakes requires modelling methane
1356 emissions from their anoxic sediment (Bastviken et al., 2004) and care needs to be taken to
1357 avoid double counting the wetland extent of inland lakes (Thornton Brett et al., 2016).

1358

1359 We have not evaluated the model's wetland methane emissions at the site level against
1360 observations. Wetland methane emissions are known to be spatially highly heterogeneous and
1361 temporally intermittent (e.g. Godwin et al., 2013) and CLASS-CTEM does not represent

Formatted: Font: (Default) Times
New Roman, 12 pt

Formatted: Font: (Default) Times
New Roman, 12 pt

1362 physical processes that govern methane emissions at small spatial and temporal scales.
1363 Instead the model is designed for operation at large spatial scales (> 100 km) and
1364 implementation within an Earth system model and as such only temperature, soil moisture
1365 and substrate availability (through heterotrophic respiration) are taken into account. Water
1366 table depth, ebullition, transport through vascular plants, and PFTs specific to wetlands are
1367 not considered in our modelling framework. The corollary of this is that our model cannot be
1368 expected to reproduce wetland methane emissions at a point scale where site specific
1369 processes and conditions including water depth, ebullition, and wetland specific PFTs
1370 become more important. Similar approaches are followed by several large scale models
1371 including a recent attempt by Bloom et al. (2017) who derive wetland methane emissions
1372 using heterotrophic respiration from eight terrestrial ecosystem models.

Deleted: and

1373
1374 We have also not evaluated parameter and forcing uncertainties in relation to simulated
1375 methane emissions. However, several aspects of the CLASS-CTEM model have been
1376 evaluated before against observations including photosynthesis, autotrophic and heterotrophic
1377 respiration, allocation of carbon from leaves to stem and root components, dynamic leaf
1378 phenology, fire, and land use change. These aspects of the model have been evaluated at
1379 point (Arora and Boer, 2005a; Melton et al., 2015), regional (Arora et al., 2016; Garnaud et
1380 al., 2015; Peng et al., 2014) and global (Arora and Boer, 2010; Melton and Arora, 2014,
1381 2016) scales. In regards to processes relevant to methane emissions from wetlands (which, of
1382 course, is the largest natural source) heterotrophic respiration and wetland extent are the most
1383 important. Uncertainties in these two quantities will propagate to calculated methane
1384 emissions from wetlands. The majority of increase in wetland methane emissions over the
1385 historical period comes from an increase in heterotrophic respiratory flux due to increase in
1386 gross and net primary productivities in response to increase in atmospheric CO₂

Deleted: ¶

Formatted: Font: (Default) Times New Roman, 12 pt

Field Code Changed

Formatted: Font: (Default) Times New Roman, 12 pt, French (Canada)

Formatted: French (Canada)

Formatted: Font: (Default) Times New Roman, 12 pt

Field Code Changed

Formatted: Subscript

1389 concentration. The rate of increase of simulated gross primary productivity is adjusted in
1390 CLASS-CTEM to obtain realistic land carbon sink from 1960 onwards (Le Quéré et al.,
1391 2018) but also to obtain a realistic amplitude of the annual CO₂ cycle in a fully coupled Earth
1392 system model simulation (Arora and Scinocca, 2016). The response of model's heterotrophic
1393 respiration to soil moisture is expressed as a function of soil matric potential as mentioned
1394 earlier in section 2.1.1.1. This response is based on Griffin (1981) who suggests that the
1395 microbial activity is optimal at an absolute soil matric potential of 0.05 MPa and decreases as
1396 the soil becomes waterlogged near 0.00 MPa or too dry near 1.5 MPa . This parameterization
1397 has been evaluated indirectly at seasonally dry locations in the Amazonia (Melton et al.,
1398 2015).

Formatted: Subscript

Formatted: Font: (Default) Times
New Roman, 12 pt

1400 Our next step to evaluate natural methane fluxes from CLASS-CTEM is to use these fluxes in
1401 an atmospheric transport model to simulate and compare methane concentrations at selected
1402 stations to assess seasonality of simulated wetland methane emissions at large spatial scales
1403 in a somewhat more direct manner. In addition, CLASS-CTEM simulated natural fluxes can
1404 be used as a prior in a methane inversion-based system, together with anthropogenic methane
1405 emissions, to calculate optimized posterior fluxes to which the prior fluxes can be compared.
1406 Although atmospheric inversions-based systems have their own limitations (Houweling et al.,
1407 2017), the objective is to evaluate CLASS-CTEM simulated natural methane fluxes using a
1408 range of available methodologies.

Deleted: .

1410 Overall the results presented here suggest that the natural fluxes of methane between the
1411 atmosphere and the land, and the geographical distribution of wetland extent, simulated by
1412 the CLASS-CTEM modelling framework are sufficiently realistic to use the model to study
1413 the changes in natural methane fluxes due to changes in environmental conditions.

1415
1416
1417
1418
1419
1420
1421
1422
1423

Acknowledgements

We would like to thank Douglas Chan and Reinel Sospedra-Alfonso for providing comments on an earlier version of this manuscript. We also thank the two anonymous reviewers for their comments and our handling editor Alexey V. Eliseev for his time and effort.

1424 References

- 1425 [Amante, C. and Eakins, B. W.: ETOPO1 1 Arc-Minute Global Relief Model: Procedures,](#)
1426 [Data Sources and Analysis. NOAA Technical Memorandum NESDIS NGDC-24, 19 pp.,](#)
1427 [doi:10.7289/V5C8276M, 2009.](#)
- 1428 [Andreae, M. O. and Merlet, P.: Emission of trace gases and aerosols from biomass burning,](#)
1429 [Glob. Biogeochem. Cycles, 15\(4\), 955–966, doi:10.1029/2000GB001382, 2001.](#)
- 1430 [Arora, V. K.: Land surface modelling in general circulation models: a hydrological](#)
1431 [perspective, PhD thesis, University of Melbourne, Melbourne, Australia., 1997.](#)
- 1432 [Arora, V. K. and Boer, G. J.: A Representation of Variable Root Distribution in Dynamic](#)
1433 [Vegetation Models, Earth Interact., 7\(6\), 1–19, doi:10.1175/1087-](#)
1434 [3562\(2003\)007<0001:AROVRD>2.0.CO;2, 2003.](#)
- 1435 [Arora, V. K. and Boer, G. J.: A parameterization of leaf phenology for the terrestrial](#)
1436 [ecosystem component of climate models, Glob. Change Biol., 11\(1\), 39–59,](#)
1437 [doi:10.1111/j.1365-2486.2004.00890.x, 2005a.](#)
- 1438 [Arora, V. K. and Boer, G. J.: Fire as an interactive component of dynamic vegetation models,](#)
1439 [J. Geophys. Res. Biogeosciences, 110\(G2\), doi:10.1029/2005JG000042, 2005b.](#)
- 1440 [Arora, V. K. and Boer, G. J.: Uncertainties in the 20th century carbon budget associated with](#)
1441 [land use change, Glob. Change Biol., 16\(12\), 3327–3348, doi:10.1111/j.1365-](#)
1442 [2486.2010.02202.x, 2010.](#)
- 1443 [Arora, V. K. and Melton, J. R.: Reduction in global area burned and wildfire emissions since](#)
1444 [1930s enhances carbon uptake by land, Nat. Commun., 9\(1\), 1326, doi:10.1038/s41467-](#)
1445 [018-03838-0, 2018.](#)
- 1446 [Arora, V. K. and Scinocca, J. F.: Constraining the strength of the terrestrial CO2 fertilization](#)
1447 [effect in the Canadian Earth system model version 4.2 \(CanESM4.2\), Geosci. Model Dev.,](#)
1448 [9\(7\), 2357–2376, doi:10.5194/gmd-9-2357-2016, 2016.](#)
- 1449 [Arora, V. K., Boer, G. J., Christian, J. R., Curry, C. L., Denman, K. L., Zahariev, K., Flato, G.](#)
1450 [M., Scinocca, J. F., Merryfield, W. J. and Lee, W. G.: The Effect of Terrestrial](#)
1451 [Photosynthesis Down Regulation on the Twentieth-Century Carbon Budget Simulated with](#)
1452 [the CCCma Earth System Model, J. Clim., 22\(22\), 6066–6088,](#)
1453 [doi:10.1175/2009JCLI3037.1, 2009.](#)
- 1454 [Arora, V. K., Scinocca, J. F., Boer, G. J., Christian, J. R., Denman, K. L., Flato, G. M.,](#)
1455 [Kharin, V. V., Lee, W. G. and Merryfield, W. J.: Carbon emission limits required to satisfy](#)
1456 [future representative concentration pathways of greenhouse gases, Geophys. Res. Lett.,](#)
1457 [38\(5\), doi:10.1029/2010GL046270, 2011.](#)
- 1458 [Arora, V. K., Boer, G. J., Friedlingstein, P., Eby, M., Jones, C. D., Christian, J. R., Bonan, G.,](#)
1459 [Bopp, L., Brovkin, V., Cadule, P., Hajima, T., Ilyina, T., Lindsay, K., Tjiputra, J. F. and Wu,](#)
1460 [T.: Carbon–Concentration and Carbon–Climate Feedbacks in CMIP5 Earth System Models,](#)
1461 [J. Clim., 26\(15\), 5289–5314, doi:10.1175/JCLI-D-12-00494.1, 2013.](#)
- 1462 [Arora, V. K., Peng, Y., Kurz, W. A., Fyfe, J. C., Hawkins, B. and Werner, A. T.: Potential](#)
1463 [near-future carbon uptake overcomes losses from a large insect outbreak in British](#)
1464 [Columbia, Canada, Geophys. Res. Lett., 43\(6\), 2590–2598, doi:10.1002/2015GL067532,](#)
1465 [2016.](#)

Formatted: Bibliography,
Widow/Orphan control, Adjust space
between Latin and Asian text, Adjust
space between Asian text and numb

1466 [Bastviken, D., Cole, J., Pace, M. and Tranvik, L.: Methane emissions from lakes:](#)
1467 [Dependence of lake characteristics, two regional assessments, and a global estimate, Glob.](#)
1468 [Biogeochem. Cycles, 18\(4\), doi: 10.1029/2004GB002238, doi:10.1029/2004GB002238,](#)
1469 [2004.](#)

1470 [Bloom, A. A., Bowman, K. W., Lee, M., Turner, A. J., Schroeder, R., Worden, J. R., Weidner,](#)
1471 [R., McDonald, K. C. and Jacob, D. J.: A global wetland methane emissions and uncertainty](#)
1472 [dataset for atmospheric chemical transport models \(WetCHARTs version 1.0\), Geosci Model](#)
1473 [Dev, 10\(6\), 2141–2156, doi:10.5194/gmd-10-2141-2017, 2017.](#)

1474 [Bohn, T. J., Melton, J. R., Ito, A., Kleinen, T., Spahni, R., Stocker, B. D., Zhang, B., Zhu, X.,](#)
1475 [Schroeder, R., Glagolev, M. V., Maksyutov, S., Brovkin, V., Chen, G., Denisov, S. N.,](#)
1476 [Eliseev, A. V., Gallego-Sala, A., McDonald, K. C., Rawlins, M. A., Riley, W. J., Subin, Z. M.,](#)
1477 [Tian, H., Zhuang, Q. and Kaplan, J. O.: WETCHIMP-WSL: intercomparison of wetland](#)
1478 [methane emissions models over West Siberia, Biogeosciences, 12\(11\), 3321–3349,](#)
1479 [doi:10.5194/bg-12-3321-2015, 2015.](#)

1480 [Bousquet, P., Ringeval, B., Pison, I., Dlugokencky, E. J., Brunke, E.-G., Carouge, C.,](#)
1481 [Chevallier, F., Fortems-Cheiney, A., Frankenberg, C., Hauglustaine, D. A., Krummel, P. B.,](#)
1482 [Langenfelds, R. L., Ramonet, M., Schmidt, M., Steele, L. P., Szopa, S., Yver, C., Viovy, N.](#)
1483 [and Ciais, P.: Source attribution of the changes in atmospheric methane for 2006–2008,](#)
1484 [Atmos Chem Phys, 11\(8\), 3689–3700, doi:10.5194/acp-11-3689-2011, 2011.](#)

1485 [Chengjin, C., Megan, B., Youshi, W., Fangliang, H., Jacob, W., Jérôme, C. and Lawren, S.:](#)
1486 [Does climate directly influence NPP globally?, Glob. Change Biol., 22\(1\), 12–24,](#)
1487 [doi:10.1111/gcb.13079, 2016.](#)

1488 [Collins, W. J., Bellouin, N., Doutriaux-Boucher, M., Gedney, N., Halloran, P., Hinton, T.,](#)
1489 [Hughes, J., Jones, C. D., Joshi, M., Liddicoat, S., Martin, G., O'Connor, F., Rae, J., Senior,](#)
1490 [C., Sitch, S., Totterdell, I., Wiltshire, A. and Woodward, S.: Development and evaluation of](#)
1491 [an Earth-System model – HadGEM2, Geosci. Model Dev., 4\(4\), 1051–1075,](#)
1492 [doi:10.5194/gmd-4-1051-2011, 2011.](#)

1493 [Curry, C. L.: Modeling the soil consumption of atmospheric methane at the global scale,](#)
1494 [Glob. Biogeochem. Cycles, 21\(4\), doi:10.1029/2006GB002818, 2007.](#)

1495 [Dalva, M., Moore, T. R., Arp, P. and Clair, T. A.: Methane and soil and plant community](#)
1496 [respiration from wetlands, Kejimikujik National Park, Nova Scotia: Measurements,](#)
1497 [predictions, and climatic change, J. Geophys. Res. Atmospheres, 106\(D3\), 2955–2962,](#)
1498 [doi:10.1029/2000JD900500, 2001.](#)

1499 [Denman, K. L., Brasseur, G., Chidthaisong, A., Ciais, P., Cox, P. M., Dickinson, R. E.,](#)
1500 [Hauglustaine, D., Heinze, C., Holland, E., Jacob, D., Lohmann, U., Ramachandran, S., da](#)
1501 [Silva Dias, P. L., Wofsy, S. C. and Zhang, H.: Couplings Between Changes in the Climate](#)
1502 [System and Biogeochemistry, in Climate Change 2007: The Physical Science Basis.](#)
1503 [Contribution of Working Group I to the Fourth Assessment Report of the Intergovernmental](#)
1504 [Panel on Climate Change \[Solomon, S., D. Qin, M. Manning, Z. Chen, M. Marquis, K.B.](#)
1505 [Averyt, M. Tignor and H.L. Miller \(eds.\)\], pp. 499–587, Cambridge University Press,](#)
1506 [Cambridge, United Kingdom and New York, NY, USA., 2007.](#)

1507 [European Commission: Wise use and conservation of wetlands. Communication from the](#)
1508 [Commission to the Council and the European Parliament, European Commission, Brussels,](#)
1509 [Belgium. \[online\] Available from: http://aei.pitt.edu/4792/1/4792.pdf \(Accessed 12 September](#)
1510 [2017\), 1995.](#)

1511 [Eyring, V., Butchart, N., Waugh, D. W., Akiyoshi, H., Austin, J., Bekki, S., Bodeker, G. E.,](#)
1512 [Boville, B. A., Brühl, C., Chipperfield, M. P., Cordero, E., Dameris, M., Deushi, M., Fioletov,](#)
1513 [V. E., Frith, S. M., Garcia, R. R., Gethelman, A., Giorgetta, M. A., Grewe, V., Jourdain, L.,](#)
1514 [Kinnison, D. E., Mancini, E., Manzini, E., Marchand, M., Marsh, D. R., Nagashima, T.,](#)
1515 [Newman, P. A., Nielsen, J. E., Pawson, S., Pitari, G., Plummer, D. A., Rozanov, E.,](#)
1516 [Schraner, M., Shepherd, T. G., Shibata, K., Stolarski, R. S., Struthers, H., Tian, W. and](#)
1517 [Yoshiki, M.: Assessment of temperature, trace species, and ozone in chemistry-climate](#)
1518 [model simulations of the recent past, J. Geophys. Res. Atmospheres, 111\(D22\), n/a-n/a,](#)
1519 [doi:10.1029/2006JD007327, 2006.](#)

1520 [Friedlingstein, P., Cox, P., Betts, R., Bopp, L., von Bloh, W., Brovkin, V., Cadule, P., Doney,](#)
1521 [S., Eby, M., Fung, I., Bala, G., John, J., Jones, C., Joos, F., Kato, T., Kawamiya, M., Knorr,](#)
1522 [W., Lindsay, K., Matthews, H. D., Raddatz, T., Rayner, P., Reick, C., Roeckner, E.,](#)
1523 [Schnitzler, K.-G., Schnur, R., Strassmann, K., Weaver, A. J., Yoshikawa, C. and Zeng, N.: Climate–Carbon Cycle Feedback Analysis: Results from the C4MIP Model Intercomparison,](#)
1524 [J. Clim., 19\(14\), 3337–3353, doi:10.1175/JCLI3800.1, 2006.](#)

1526 [Friedlingstein, P., Meinshausen, M., Arora, V. K., Jones, C. D., Anav, A., Liddicoat, S. K. and](#)
1527 [Knutti, R.: Uncertainties in CMIP5 Climate Projections due to Carbon Cycle Feedbacks, J.](#)
1528 [Clim., 27\(2\), 511–526, doi:10.1175/JCLI-D-12-00579.1, 2014.](#)

1529 [Garnaud, C., Sushama, L. and Versegny, D.: Impact of interactive vegetation phenology on](#)
1530 [the Canadian RCM simulated climate over North America, Clim. Dyn., 45\(5\), 1471–1492,](#)
1531 [doi:10.1007/s00382-014-2397-9, 2015.](#)

1532 [Giglio, L., Randerson, J. T. and van der Werf, G. R.: Analysis of daily, monthly, and annual](#)
1533 [burned area using the fourth-generation global fire emissions database \(GFED4\), J.](#)
1534 [Geophys. Res. Biogeosciences, 118\(1\), 317–328, doi:10.1002/jgrg.20042, 2013.](#)

1535 [Glagolev, M. V., Kleptsova, I. E., Filippov, I. V., Kazantsev, V. S., Machida, T. and](#)
1536 [Maksyutov, S. S.: Methane emissions from subtaiga mires of Western Siberia: The “standard](#)
1537 [model” Bc5, Mosc. Univ. Soil Sci. Bull., 65\(2\), 86–93, doi:10.3103/S0147687410020067,](#)
1538 [2010.](#)

1539 [Godwin, C. M., McNamara, P. J. and Markfort, C. D.: Evening methane emission pulses](#)
1540 [from a boreal wetland correspond to convective mixing in hollows, J. Geophys. Res.](#)
1541 [Biogeosciences, 118\(3\), 994–1005, doi:10.1002/jgrg.20082, 2013.](#)

1542 [Griffin, D. M.: Water potential as a selective factor in the microbial ecology of soils, in Water](#)
1543 [Potential Relations in Soil Microbiology edited by: Parr, J., Gardner, W., and Elliott, L., pp.](#)
1544 [141–151, Soil Sci. Soc. Am., 1981.](#)

1545 [Houweling, S., Bergamaschi, P., Chevallier, F., Heimann, M., Kaminski, T., Krol, M.,](#)
1546 [Michalak, A. M. and Patra, P.: Global inverse modeling of CH₄ sources and sinks: an](#)
1547 [overview of methods, Atmos Chem Phys, 17\(1\), 235–256, doi:10.5194/acp-17-235-2017,](#)
1548 [2017.](#)

1549 [Hurt, G. C., Frolking, S., Fearon, M. G., Moore, B., Shevliakova, E., Malyshev, S., Pacala,](#)
1550 [S. W. and Houghton, R. A.: The underpinnings of land-use history: three centuries of global](#)
1551 [gridded land-use transitions, wood-harvest activity, and resulting secondary lands, Glob.](#)
1552 [Change Biol., 12\(7\), 1208–1229, doi:10.1111/j.1365-2486.2006.01150.x, 2006.](#)

1553 [Jones, C., Robertson, E., Arora, V., Friedlingstein, P., Shevliakova, E., Bopp, L., Brovkin, V.,](#)
1554 [Hajima, T., Kato, E., Kawamiya, M., Liddicoat, S., Lindsay, K., Reick, C. H., Roelandt, C.,](#)
1555 [Segsneider, J. and Tjiputra, J.: Twenty-First-Century Compatible CO₂ Emissions and](#)

1556 [Airborne Fraction Simulated by CMIP5 Earth System Models under Four Representative](#)
1557 [Concentration Pathways, J. Clim., 26\(13\), 4398–4413, doi:10.1175/JCLI-D-12-00554.1,](#)
1558 [2013.](#)

1559 [Kaplan, J. O.: Wetlands at the Last Glacial Maximum: Distribution and methane emissions,](#)
1560 [Geophys. Res. Lett., 29\(6\), 3–1, doi:10.1029/2001GL013366, 2002.](#)

1561 [Kim, H.-S., Maksyutov, S., Glagolev, M. V., Machida, T., Patra, P. K., Sudo, K. and Inoue,](#)
1562 [G.: Evaluation of methane emissions from West Siberian wetlands based on inverse](#)
1563 [modeling, Environ. Res. Lett., 6\(3\), 035201, 2011.](#)

1564 [Kloster, S., Mahowald, N. M., Randerson, J. T., Thornton, P. E., Hoffman, F. M., Levis, S.,](#)
1565 [Lawrence, P. J., Feddesma, J. J., Oleson, K. W. and Lawrence, D. M.: Fire dynamics during](#)
1566 [the 20th century simulated by the Community Land Model, Biogeosciences, 7\(6\), 1877–](#)
1567 [1902, doi:10.5194/bg-7-1877-2010, 2010.](#)

1568 [Lamarque, J.-F., Bond, T. C., Eyring, V., Granier, C., Heil, A., Klimont, Z., Lee, D., Liousse,](#)
1569 [C., Mieville, A., Owen, B., Schultz, M. G., Shindell, D., Smith, S. J., Stehfest, E., Van](#)
1570 [Aardenne, J., Cooper, O. R., Kainuma, M., Mahowald, N., McConnell, J. R., Naik, V., Riahi,](#)
1571 [K. and van Vuuren, D. P.: Historical \(1850–2000\) gridded anthropogenic and biomass](#)
1572 [burning emissions of reactive gases and aerosols: methodology and application,](#)
1573 [Atmospheric Chem. Phys., 10\(15\), 7017–7039, doi:10.5194/acp-10-7017-2010, 2010.](#)

1574 [Lamarque, J.-F., Shindell, D. T., Josse, B., Young, P. J., Cionni, I., Eyring, V., Bergmann, D.,](#)
1575 [Cameron-Smith, P., Collins, W. J., Doherty, R., Dalsoren, S., Faluvegi, G., Folberth, G.,](#)
1576 [Ghan, S. J., Horowitz, L. W., Lee, Y. H., MacKenzie, I. A., Nagashima, T., Naik, V.,](#)
1577 [Plummer, D., Righi, M., Rumbold, S. T., Schulz, M., Skeie, R. B., Stevenson, D. S., Strode,](#)
1578 [S., Sudo, K., Szopa, S., Voulgarakis, A. and Zeng, G.: The Atmospheric Chemistry and](#)
1579 [Climate Model Intercomparison Project \(ACCMIP\): overview and description of models,](#)
1580 [simulations and climate diagnostics, Geosci. Model Dev., 6\(1\), 179–206, doi:10.5194/gmd-6-](#)
1581 [179-2013, 2013.](#)

1582 [Langer, M., Westermann, S., Walter Anthony, K., Wischniewski, K. and Boike, J.: Frozen](#)
1583 [ponds: production and storage of methane during the Arctic winter in a lowland tundra](#)
1584 [landscape in northern Siberia, Lena River delta, Biogeosciences, 12\(4\), 977–990,](#)
1585 [doi:10.5194/bg-12-977-2015, 2015.](#)

1586 [Le Quéré, C., Andrew, R. M., Friedlingstein, P., Sitch, S., Pongratz, J., Manning, A. C.,](#)
1587 [Korsbakken, J. I., Peters, G. P., Canadell, J. G., Jackson, R. B., Boden, T. A., Tans, P. P.,](#)
1588 [Andrews, O. D., Arora, V. K., Bakker, D. C. E., Barbero, L., Becker, M., Betts, R. A., Bopp,](#)
1589 [L., Chevallier, F., Chini, L. P., Ciais, P., Cosca, C. E., Cross, J., Currie, K., Gasser, T.,](#)
1590 [Harris, I., Hauck, J., Haverd, V., Houghton, R. A., Hunt, C. W., Hurtt, G., Ilyina, T., Jain, A.](#)
1591 [K., Kato, E., Kautz, M., Keeling, R. F., Klein Goldewijk, K., Körtzinger, A., Landschützer, P.,](#)
1592 [Lefèvre, N., Lenton, A., Lienert, S., Lima, I., Lombardozzi, D., Metzl, N., Millero, F., Monteiro,](#)
1593 [P. M. S., Munro, D. R., Nabel, J. E. M. S., Nakaoka, S.-I., Nojiri, Y., Padin, X. A., Peregon,](#)
1594 [A., Pfeil, B., Pierrot, D., Poulter, B., Rehder, G., Reimer, J., Rödenbeck, C., Schwinger, J.,](#)
1595 [Séférian, R., Skjelvan, I., Stocker, B. D., Tian, H., Tilbrook, B., Tubiello, F. N., van der Laan-](#)
1596 [Luijkx, I. T., van der Werf, G. R., van Heuven, S., Viovy, N., Vuichard, N., Walker, A. P.,](#)
1597 [Watson, A. J., Wiltshire, A. J., Zaehle, S. and Zhu, D.: Global Carbon Budget 2017, Earth](#)
1598 [Syst. Sci. Data, 10\(1\), 405–448, doi:10.5194/essd-10-405-2018, 2018.](#)

1599 [Lehner, B. and Döll, P.: Development and validation of a global database of lakes, reservoirs](#)
1600 [and wetlands, J. Hydrol., 296\(1–4\), 1–22, doi:10.1016/j.jhydrol.2004.03.028, 2004.](#)

1601 [Li, F., Zeng, X. D. and Levis, S.: A process-based fire parameterization of intermediate](#)
1602 [complexity in a Dynamic Global Vegetation Model, Biogeosciences Discuss., 9\(3\), 3233–](#)
1603 [3287, doi:10.5194/bgd-9-3233-2012, 2012.](#)

1604 [Marlon, J. R., Bartlein, P. J., Carcaillet, C., Gavin, D. G., Harrison, S. P., Higuera, P. E.,](#)
1605 [Joos, F., Power, M. J. and Prentice, I. C.: Climate and human influences on global biomass](#)
1606 [burning over the past two millennia, Nat. Geosci, 1\(10\), 697–702, doi:10.1038/ngeo313,](#)
1607 [2008.](#)

1608 [Matthes, K., Funke, B., Andersson, M. E., Barnard, L., Beer, J., Charbonneau, P., Clilverd,](#)
1609 [M. A., Dudok de Wit, T., Haberreiter, M., Hendry, A., Jackman, C. H., Kretzschmar, M.,](#)
1610 [Kruschke, T., Kunze, M., Langematz, U., Marsh, D. R., Maycock, A. C., Misios, S., Rodger,](#)
1611 [C. J., Scaife, A. A., Seppälä, A., Shangguan, M., Sinnhuber, M., Tourpali, K., Usoskin, I., van](#)
1612 [de Kamp, M., Verronen, P. T. and Versick, S.: Solar forcing for CMIP6 \(v3.2\), Geosci. Model](#)
1613 [Dev., 10\(6\), 2247–2302, doi:10.5194/gmd-10-2247-2017, 2017.](#)

1614 [Matthews, E. and Fung, I.: Methane emission from natural wetlands: Global distribution,](#)
1615 [area, and environmental characteristics of sources, Glob. Biogeochem. Cycles, 1\(1\), 61–86,](#)
1616 [doi:10.1029/GB001i001p00061, 1987.](#)

1617 [Meinshausen, M., Smith, S. J., Calvin, K., Daniel, J. S., Kainuma, M. L. T., Lamarque, J.-F.,](#)
1618 [Matsumoto, K., Montzka, S. A., Raper, S. C. B., Riahi, K., Thomson, A., Velders, G. J. M.](#)
1619 [and van Vuuren, D. P. P.: The RCP greenhouse gas concentrations and their extensions](#)
1620 [from 1765 to 2300, Clim. Change, 109\(1\), 213, doi:10.1007/s10584-011-0156-z, 2011.](#)

1621 [Melton, J. R. and Arora, V. K.: Sub-grid scale representation of vegetation in global land](#)
1622 [surface schemes: implications for estimation of the terrestrial carbon sink, Biogeosciences,](#)
1623 [11\(4\), 1021–1036, doi:10.5194/bg-11-1021-2014, 2014.](#)

1624 [Melton, J. R. and Arora, V. K.: Competition between plant functional types in the Canadian](#)
1625 [Terrestrial Ecosystem Model \(CTEM\) v. 2.0, Geosci Model Dev, 9\(1\), 323–361,](#)
1626 [doi:10.5194/gmd-9-323-2016, 2016.](#)

1627 [Melton, J. R., Wania, R., Hodson, E. L., Poulter, B., Ringeval, B., Spahni, R., Bohn, T., Avis,](#)
1628 [C. A., Beerling, D. J., Chen, G., Eliseev, A. V., Denisov, S. N., Hopcroft, P. O., Lettenmaier,](#)
1629 [D. P., Riley, W. J., Singarayer, J. S., Subin, Z. M., Tian, H., Zürcher, S., Brovkin, V., van](#)
1630 [Bodegom, P. M., Kleinen, T., Yu, Z. C. and Kaplan, J. O.: Present state of global wetland](#)
1631 [extent and wetland methane modelling: conclusions from a model inter-comparison project](#)
1632 [\(WETCHIMP\), Biogeosciences, 10\(2\), 753–788, doi:10.5194/bg-10-753-2013, 2013.](#)

1633 [Melton, J. R., Shrestha, R. K. and Arora, V. K.: The influence of soils on heterotrophic](#)
1634 [respiration exerts a strong control on net ecosystem productivity in seasonally dry](#)
1635 [Amazonian forests, Biogeosciences, 12\(4\), 1151–1168, doi:10.5194/bg-12-1151-2015,](#)
1636 [2015.](#)

1637 [Migliavacca, M., Dosio, A., Kloster, S., Ward, D. S., Camia, A., Houborg, R., Houston](#)
1638 [Durrant, T., Khabarov, N., Krasovskii, A. A., San Miguel-Ayanz, J. and Cescatti, A.: Modeling](#)
1639 [burned area in Europe with the Community Land Model, J. Geophys. Res. Biogeosciences,](#)
1640 [118\(1\), 265–279, doi:10.1002/jgrg.20026, 2013.](#)

1641 [Myhre, G., Shindell, D., Bréon, F.-M., Collins, W., Fuglestad, J., Huang, J., Koch, D.,](#)
1642 [Lamarque, J.-F., Lee, D., Mendoza, B., Nakajima, T., Robock, A., Stephens, G., Takemura,](#)
1643 [T. and Zhang, H.: Anthropogenic and Natural Radiative Forcing, in Climate Change 2013:](#)
1644 [The Physical Science Basis. Contribution of Working Group I to the Fifth Assessment Report](#)
1645 [of the Intergovernmental Panel on Climate Change, edited by T. F. Stocker, D. Qin, G.-K.](#)

1646 [Plattner, M. Tignor, S. K. Allen, J. Boschung, A. Nauels, Y. Xia, V. Bex, and P. M. Midgley,](#)
1647 [pp. 659–740, Cambridge University Press, Cambridge, United Kingdom and New York, NY,](#)
1648 [USA., 2013.](#)

1649 [Naik, V., Voulgarakis, A., Fiore, A. M., Horowitz, L. W., Lamarque, J.-F., Lin, M., Prather, M.](#)
1650 [J., Young, P. J., Bergmann, D., Cameron-Smith, P. J., Cionni, I., Collins, W. J., Dalsøren, S.](#)
1651 [B., Doherty, R., Eyring, V., Faluvegi, G., Folberth, G. A., Josse, B., Lee, Y. H., MacKenzie, I.](#)
1652 [A., Nagashima, T., van Noije, T. P. C., Plummer, D. A., Righi, M., Rumbold, S. T., Skeie, R.,](#)
1653 [Shindell, D. T., Stevenson, D. S., Strode, S., Sudo, K., Szopa, S. and Zeng, G.: Preindustrial](#)
1654 [to present-day changes in tropospheric hydroxyl radical and methane lifetime from the](#)
1655 [Atmospheric Chemistry and Climate Model Intercomparison Project \(ACCMIP\), Atmospheric](#)
1656 [Chem. Phys., 13\(10\), 5277–5298, doi:10.5194/acp-13-5277-2013, 2013.](#)

1657 [Neely III, R. R., Conley, A. J., Vitt, F. and Lamarque, J.-F.: A consistent prescription of](#)
1658 [stratospheric aerosol for both radiation and chemistry in the Community Earth System Model](#)
1659 [\(CESM1\), Geosci. Model Dev., 9\(7\), 2459–2470, doi:10.5194/gmd-9-2459-2016, 2016.](#)

1660 [Papa, F., Prigent, C., Aires, F., Jimenez, C., Rossow, W. B. and Matthews, E.: Interannual](#)
1661 [variability of surface water extent at the global scale, 1993–2004, J. Geophys. Res.](#)
1662 [Atmospheres, 115\(D12\), n/a-n/a, doi:10.1029/2009JD012674, 2010.](#)

1663 [Peng, Y., Arora, V. K., Kurz, W. A., Hember, R. A., Hawkins, B. J., Fyfe, J. C. and Werner,](#)
1664 [A. T.: Climate and atmospheric drivers of historical terrestrial carbon uptake in the province](#)
1665 [of British Columbia, Canada, Biogeosciences, 11\(3\), 635–649, doi:10.5194/bg-11-635-2014,](#)
1666 [2014.](#)

1667 [Peregon, A., Maksyutov, S. and Yamagata, Y.: An image-based inventory of the spatial](#)
1668 [structure of West Siberian wetlands, Environ. Res. Lett., 4\(4\), 045014, 2009.](#)

1669 [Poulter, B., Bousquet, P., Canadell, J. G., Ciais, P., Peregon, A., Marielle Saunois, Arora, V.](#)
1670 [K., Beerling, D. J., Brovkin, V., Jones, C. D., Joos, F., Nicola Gedney, Ito, A., Kleinen, T.,](#)
1671 [Koven, C. D., McDonald, K., Melton, J. R., Peng, C., Shushi Peng, Prigent, C., Schroeder,](#)
1672 [R., Riley, W. J., Saito, M., Spahni, R., Tian, H., Lyla Taylor, Viovy, N., Wilton, D., Wiltshire,](#)
1673 [A., Xu, X., Zhang, B., Zhang, Z. and Zhu, Q.: Global wetland contribution to 2000–2012](#)
1674 [atmospheric methane growth rate dynamics, Environ. Res. Lett., 12\(9\), 094013, 2017.](#)

1675 [Prather, M. J., Holmes, C. D. and Hsu, J.: Reactive greenhouse gas scenarios: Systematic](#)
1676 [exploration of uncertainties and the role of atmospheric chemistry, Geophys. Res. Lett.,](#)
1677 [39\(9\), n/a-n/a, doi:10.1029/2012GL051440, 2012.](#)

1678 [Prigent, C., Papa, F., Aires, F., Rossow, W. B. and Matthews, E.: Global inundation](#)
1679 [dynamics inferred from multiple satellite observations, 1993–2000, J. Geophys. Res.](#)
1680 [Atmospheres, 112\(D12\), n/a-n/a, doi:10.1029/2006JD007847, 2007.](#)

1681 [Randerson, J. T., Chen, Y., van der Werf, G. R., Rogers, B. M. and Morton, D. C.: Global](#)
1682 [burned area and biomass burning emissions from small fires, J. Geophys. Res.](#)
1683 [Biogeosciences, 117\(G4\), n/a-n/a, doi:10.1029/2012JG002128, 2012.](#)

1684 [Saunois, M., Bousquet, P., Poulter, B., Peregon, A., Ciais, P., Canadell, J. G., Dlugokencky,](#)
1685 [E. J., Etiope, G., Bastviken, D., Houweling, S., Janssens-Maenhout, G., Tubiello, F. N.,](#)
1686 [Castaldi, S., Jackson, R. B., Alexe, M., Arora, V. K., Beerling, D. J., Bergamaschi, P., Blake,](#)
1687 [D. R., Brailsford, G., Brovkin, V., Bruhwiler, L., Crevoisier, C., Crill, P., Covey, K., Curry, C.,](#)
1688 [Frankenberg, C., Gedney, N., Höglund-Isaksson, L., Ishizawa, M., Ito, A., Joos, F., Kim, H.-](#)
1689 [S., Kleinen, T., Krummel, P., Lamarque, J.-F., Langenfelds, R., Locatelli, R., Machida, T.,](#)
1690 [Maksyutov, S., McDonald, K. C., Marshall, J., Melton, J. R., Morino, I., Naik, V., O'Doherty,](#)

1691 [S., Parmentier, F.-J. W., Patra, P. K., Peng, C., Peng, S., Peters, G. P., Pison, I., Prigent, C.,](#)
 1692 [Prinn, R., Ramonet, M., Riley, W. J., Saito, M., Santini, M., Schroeder, R., Simpson, I. J.,](#)
 1693 [Spahni, R., Steele, P., Takizawa, A., Thornton, B. F., Tian, H., Tohjima, Y., Viovy, N.,](#)
 1694 [Voulgarakis, A., van Weele, M., van der Werf, G. R., Weiss, R., Wiedinmyer, C., Wilton, D.](#)
 1695 [J., Wiltshire, A., Worthy, D., Wunch, D., Xu, X., Yoshida, Y., Zhang, B., Zhang, Z. and Zhu,](#)
 1696 [Q.: The global methane budget 2000–2012, Earth Syst Sci Data, 8\(2\), 697–751,](#)
 1697 [doi:10.5194/essd-8-697-2016, 2016.](#)

1698 [Schroeder, R., McDonald, C. K., Chapman, D. B., Jensen, K., Podest, E., Tessler, D. Z.,](#)
 1699 [Bohn, J. T. and Zimmermann, R.: Development and Evaluation of a Multi-Year Fractional](#)
 1700 [Surface Water Data Set Derived from Active/Passive Microwave Remote Sensing Data,](#)
 1701 [Remote Sens., 7\(12\), doi:10.3390/rs71215843, 2015.](#)

1702 [Scinocca, J. F., McFarlane, N. A., Lazare, M., Li, J. and Plummer, D.: Technical Note: The](#)
 1703 [CCCma third generation AGCM and its extension into the middle atmosphere, Atmospheric](#)
 1704 [Chem. Phys., 8\(23\), 7055–7074, doi:10.5194/acp-8-7055-2008, 2008.](#)

1705 [Shindell, D., Kuylensstierna, J. C. I., Vignati, E., van Dingenen, R., Amann, M., Klimont, Z.,](#)
 1706 [Anenberg, S. C., Muller, N., Janssens-Maenhout, G., Raes, F., Schwartz, J., Faluvegi, G.,](#)
 1707 [Pozzoli, L., Kupiainen, K., Höglund-Isaksson, L., Emberson, L., Streets, D., Ramanathan, V.,](#)
 1708 [Hicks, K., Oanh, N. T. K., Milly, G., Williams, M., Demkine, V. and Fowler, D.:](#)
 1709 [Simultaneously Mitigating Near-Term Climate Change and Improving Human Health and](#)
 1710 [Food Security, Science, 335\(6065\), 183–189, 2012.](#)

1711 [Shindell, D. T., Pechony, O., Voulgarakis, A., Faluvegi, G., Nazarenko, L., Lamarque, J.-F.,](#)
 1712 [Bowman, K., Milly, G., Kovari, B., Ruedy, R. and Schmidt, G. A.: Interactive ozone and](#)
 1713 [methane chemistry in GISS-E2 historical and future climate simulations, Atmos Chem Phys,](#)
 1714 [13\(5\), 2653–2689, doi:10.5194/acp-13-2653-2013, 2013.](#)

1715 [SPARC CCMVal: SPARC Report on the Evaluation of Chemistry-Climate Models, V. Eyring,](#)
 1716 [T. G. Shepherd, D. W. Waugh \(Eds.\), SPARC Report No. 5, WCRP-132, WMO/TD-No.](#)
 1717 [1526., 2010.](#)

1718 [Thornton Brett, F., Wik, M. and Carill Patrick, M.: Double-counting challenges the accuracy](#)
 1719 [of high-latitude methane inventories, Geophys. Res. Lett., 43\(24\), 12,569–12,577,](#)
 1720 [doi:10.1002/2016GL071772, 2016.](#)

1721 [Versegny, D. L.: Class—A Canadian land surface scheme for GCMS. I. Soil model, Int. J.](#)
 1722 [Climatol., 11\(2\), 111–133, doi:10.1002/joc.3370110202, 1991.](#)

1723 [Versegny, D. L.: The Canadian land surface scheme \(CLASS\): Its history and future,](#)
 1724 [Atmosphere-Ocean, 38\(1\), 1–13, doi:10.1080/07055900.2000.9649637, 2000.](#)

1725 [Versegny, D. L., McFarlane, N. A. and Lazare, M.: Class—A Canadian land surface scheme](#)
 1726 [for GCMS, II. Vegetation model and coupled runs, Int. J. Climatol., 13\(4\), 347–370,](#)
 1727 [doi:10.1002/joc.3370130402, 1993.](#)

1728 [Viovy, N.: CRU-NCEP reanalysis data version 4, \[online\] Available from:](#)
 1729 [http://dods.extra.cea.fr/store/p529viov/cruncep/V4_1901_2012/, 2012.](#)

1730 [Voulgarakis, A., Naik, V., Lamarque, J.-F., Shindell, D. T., Young, P. J., Prather, M. J., Wild,](#)
 1731 [O., Field, R. D., Bergmann, D., Cameron-Smith, P., Cionni, I., Collins, W. J., Dalsøren, S. B.,](#)
 1732 [Doherty, R. M., Eyring, V., Faluvegi, G., Folberth, G. A., Horowitz, L. W., Josse, B.,](#)
 1733 [MacKenzie, I. A., Nagashima, T., Plummer, D. A., Righi, M., Rumbold, S. T., Stevenson, D.](#)
 1734 [S., Strode, S. A., Sudo, K., Szopa, S. and Zeng, G.: Analysis of present day and future OH](#)

1735 [and methane lifetime in the ACCMIP simulations, Atmos Chem Phys, 13\(5\), 2563–2587,](#)
1736 [doi:10.5194/acp-13-2563-2013, 2013.](#)

1737 [Walter, B. P. and Heimann, M.: A process-based, climate-sensitive model to derive methane](#)
1738 [emissions from natural wetlands: Application to five wetland sites, sensitivity to model](#)
1739 [parameters, and climate, Glob. Biogeochem. Cycles, 14\(3\), 745–765,](#)
1740 [doi:10.1029/1999GB001204, 2000.](#)

1741 [Wania, R., Ross, I. and Prentice, I. C.: Implementation and evaluation of a new methane](#)
1742 [model within a dynamic global vegetation model: LPJ-WHyMe v1.3.1, Geosci Model Dev,](#)
1743 [3\(2\), 565–584, doi:10.5194/gmd-3-565-2010, 2010.](#)

1744 [Winderlich, J.: Setup of a CO₂ and CH₄ measurement system in Central Siberia and](#)
1745 [modeling of its results, Max-Planck-Institut für Biogeochemie, Jena. \[online\] Available from:](#)
1746 [http://ediss.sub.uni-hamburg.de/volltexte/2012/5533/pdf/Dissertation.pdf, 2012.](#)

1747 [Young, P. J., Archibald, A. T., Bowman, K. W., Lamarque, J.-F., Naik, V., Stevenson, D. S.,](#)
1748 [Tilmes, S., Voulgarakis, A., Wild, O., Bergmann, D., Cameron-Smith, P., Cionni, I., Collins,](#)
1749 [W. J., Dalsøren, S. B., Doherty, R. M., Eyring, V., Faluvegi, G., Horowitz, L. W., Josse, B.,](#)
1750 [Lee, Y. H., MacKenzie, I. A., Nagashima, T., Plummer, D. A., Righi, M., Rumbold, S. T.,](#)
1751 [Skeie, R. B., Shindell, D. T., Strode, S. A., Sudo, K., Szopa, S. and Zeng, G.: Pre-industrial](#)
1752 [to end 21st century projections of tropospheric ozone from the Atmospheric Chemistry and](#)
1753 [Climate Model Intercomparison Project \(ACCMIP\), Atmospheric Chem. Phys., 13\(4\), 2063–](#)
1754 [2090, doi:10.5194/acp-13-2063-2013, 2013.](#)

1755 [Zhu, Q., Liu, J., Peng, C., Chen, H., Fang, X., Jiang, H., Yang, G., Zhu, D., Wang, W. and](#)
1756 [Zhou, X.: Modelling methane emissions from natural wetlands by development and](#)
1757 [application of the TRIPLEX-GHG model, Geosci Model Dev, 7\(3\), 981–999,](#)
1758 [doi:10.5194/gmd-7-981-2014, 2014a.](#)

1759 [Zhu, X., Zhuang, Q., Lu, X. and Song, L.: Spatial scale-dependent land–atmospheric](#)
1760 [methane exchanges in the northern high latitudes from 1993 to 2004, Biogeosciences, 11\(7\),](#)
1761 [1693–1704, doi:10.5194/bg-11-1693-2014, 2014b.](#)

1762 [Zobler, L.: A World Soil File for Global Climate Modelling, NASA Technical Memorandum](#)
1763 [87802, NASA Goddard Institute for Space Studies, New York, USA., 1986.](#)

1764 [Zona, D., Gioli, B., Commane, R., Lindaas, J., Wofsy, S. C., Miller, C. E., Dinardo, S. J.,](#)
1765 [Dengel, S., Sweeney, C., Karion, A., Chang, R. Y.-W., Henderson, J. M., Murphy, P. C.,](#)
1766 [Goodrich, J. P., Moreaux, V., Liljedahl, A., Watts, J. D., Kimball, J. S., Lipson, D. A. and](#)
1767 [Oechel, W. C.: Cold season emissions dominate the Arctic tundra methane budget, Proc.](#)
1768 [Natl. Acad. Sci., 113\(1\), 40–45, 2016.](#)

1769

1770

1771
1772
1773
1774
1775

Table 1: Emissions categories for EDGAR and RCP anthropogenic methane emissions.

EDGAR	RCP
Non-biomass burning categories	
<div>1. Energy manufacturing transformation</div> <div>2. Non-road transportation</div> <div>3. Road transportation</div> <div>4. Residential</div> <div>5. Fugitive from solid</div> <div>6. Oil production and refineries</div> <div>7. Gas production and distribution</div> <div>8. Industrial processes and product use</div> <div>9. Enteric fermentation</div> <div>10. Manure management</div> <div>11. Agricultural soils</div> <div>12. Agricultural waste burning</div> <div>13. Soil waste disposal</div> <div>14. Waste water</div> <div>15. Fossil fuel fires</div>	<div>1. Agricultural sector</div> <div>2. Agricultural waste burning</div> <div>3. Residential and commercial combustion</div> <div>4. Energy production and distribution</div> <div>5. Industrial processes and combustion</div> <div>6. Land transport emissions</div> <div>7. Waste treatment and disposal</div> <div>8. Shipping</div>
Biomass burning categories	
<div>16. Large scale biomass burning</div>	<div>9. Biomass burning from forest fires</div> <div>10. Biomass burning from grass fires</div>

1776
1777

Moved down [4]: Table 1: The upper and lower soil wetness thresholds for the latitudinal bands used in equation (1) to determine fractional wetland coverage in given grid cell.

Deleted: 2

Deleted: 3

Table 2: Comparison of CLASS-CTEM simulated annual methane emissions and annual maximum wetland extent for the West Siberia lowlands (WSL) region with models participating in the WETCHIMP-WSL intercomparison and observation- and inversion-based estimates as discussed in section 3.5. Numbers shown are mean \pm standard error from Bohn et al. (2015) for models participating in the WETCHIMP-WSL intercomparison. Standard error is not available for all inversions. All values are reported as average for the period 1993-2004 unless otherwise noted.

WSL annual maximum wetland extent (million km ²)	
Model mean from participating models in the WETCHIMP-WSL Intercomparison	0.70 \pm 0.15
CLASS-CTEM (this study)	0.53
GIEMS inundation data set	0.21
SWAMPS inundation data set	0.15
SWAMPS and GCP product (for period 2002-2012)	0.55
Peregon et al. (2009)	0.68
WSL annual wetland emissions (Tg CH ₄ /yr)	
Model mean from participating models in the WETCHIMP-WSL Intercomparison	5.34 \pm 0.54
CLASS-CTEM (this study)	7.76
Bousquet 2011 K	7.06
Bousquet 2011 R	7.13
Kim 2011 (for year 2005)	3.08 \pm 1.40
Winderlich 2012 (for year 2009)	9.80

1799
1800
1801
1802
1803
1804
1805
1806

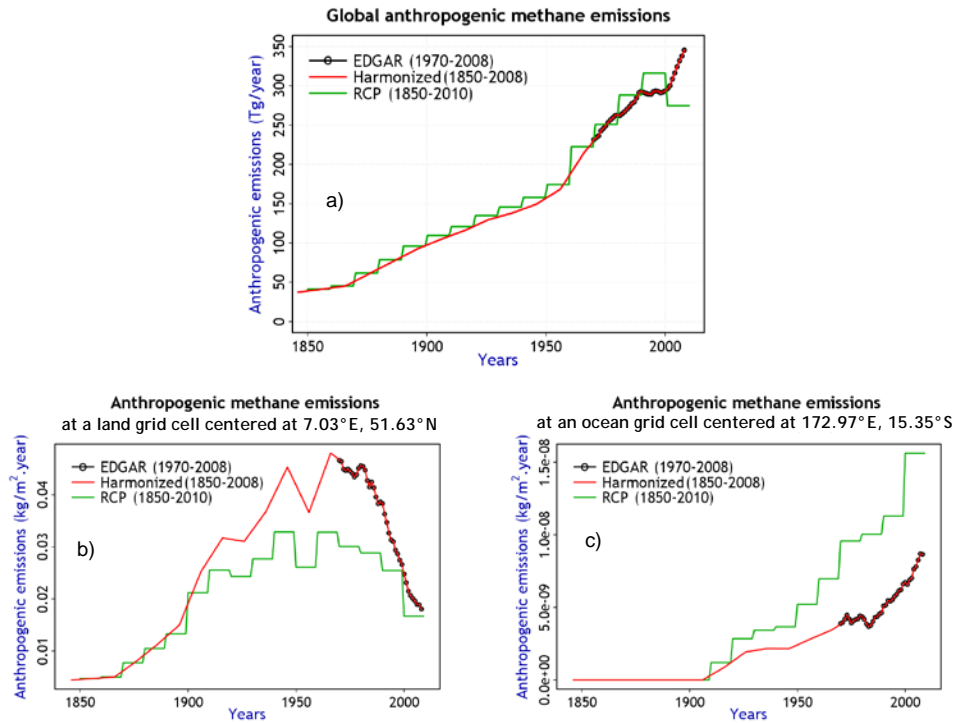
Table 3: Comparison of the components of the present day methane budget based on this study with those from Saunois et al. (2016) (based on synthesis of published studies). The values used in this study are averaged for the period 2000-2008 (since the last year of the version of EDGAR emissions used is 2008) while Saunois et al. (2016) values correspond to the 2000-2009 period.

Deleted: 4
Field Code Changed
Field Code Changed

	Saunois et al. (2016) estimates based on top-down approaches	Values used in this study and how they were obtained.	
<i>Natural sources</i>	234 [194-292]	199	
Natural wetlands	166 [125-204]	169	CLASS-CTEM simulated
Other natural sources (termites, geological, fresh water etc.)	68 [21-130]	30	Specified as a constant over the historical period
<i>Anthropogenic sources</i>	319 [255-357]	344	
Agriculture and waste	183 [112-241]	200	EDGAR
Fossil fuels	101 [77-126]	117	EDGAR
Biomass and biofuel burning	35 [16-53]	27	CLASS-CTEM simulated
<i>Sum of all sources</i>	552 [535-566]	543	
<i>Sum of all sinks</i>	546	538	
Atmospheric sink	514	509	Based on specified bias-corrected atmospheric CH4 lifetimes from CMAM
Soil sink	32 [27-38]	29	CLASS-CTEM simulated

1807
1808
1809
1810
1811
1812
1813

1815
1816
1817
1818



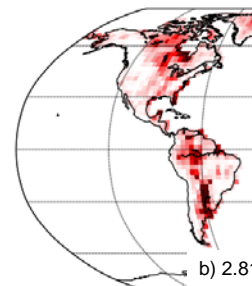
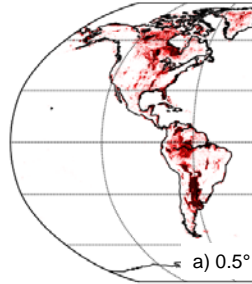
1819

1820 | Figure 1: Comparison of RCP, EDGAR and their harmonized annual global anthropogenic
1821 methane emissions (panel a) excluding biomass burning. Panels (b) and (c) illustrate the
1822 harmonization technique for a land and an ocean grid cell, respectively.

1823

Deleted: ¶

Grid cell fraction with slope
become a wetland



0.00 0.20 0.40

Figure 1: Fraction of grid cell with slope less than the threshold of 0.002 (i.e. 0.2% slope) at a) 0.5° and b) 2.81° spatial resolutions, respectively. ¶

Page Break

Moved down [3]: ¶

Deleted: 4

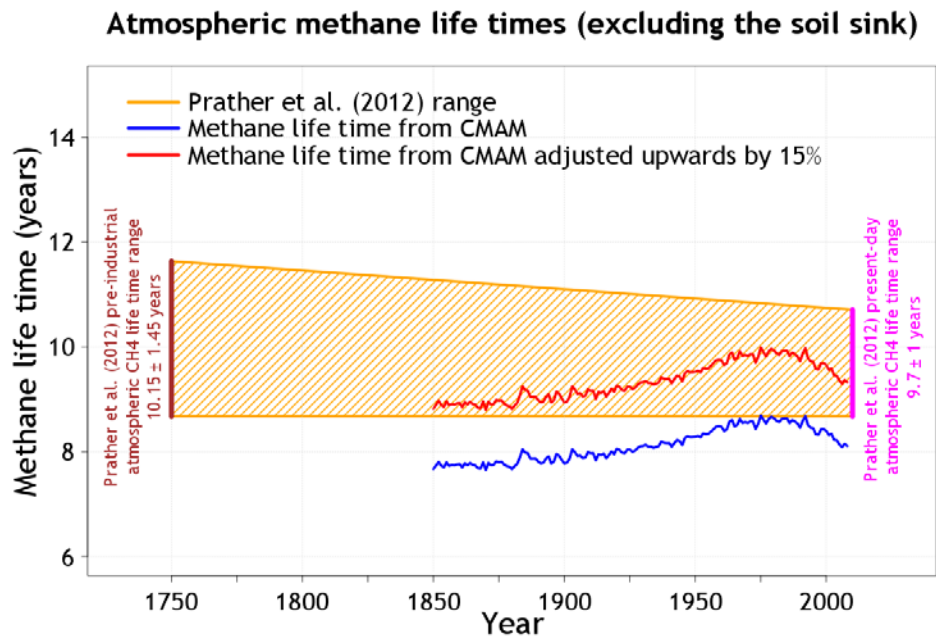
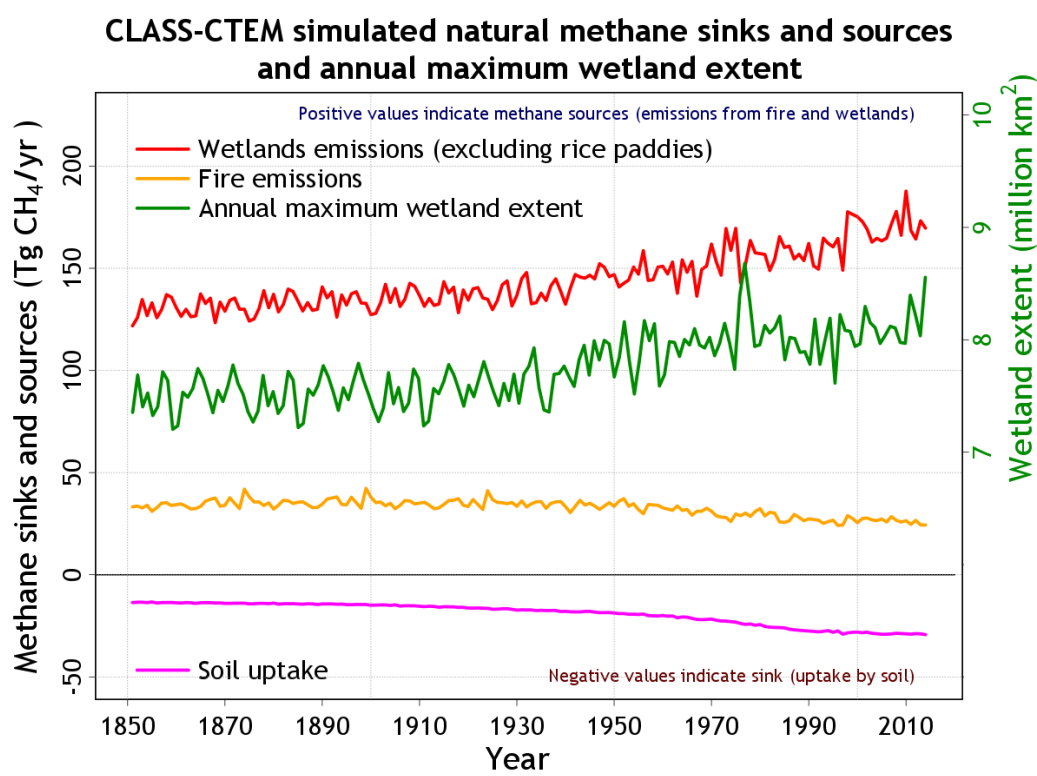


Figure 2: Comparison of atmospheric methane lifetime obtained from the Canadian Middle Atmosphere Model (CMAM) for the period 1850-2010 with observation-based estimates from Prather et al. (2012) but excluding the soil sink as explained in section 2.2.3.

Deleted: 5

1876
1877
1878



1879
1880
1881
1882
1883
1884

Figure 3: Time evolution of simulated natural methane fluxes (shown on the primary y-axis) and annual maximum wetland extent (shown on the secondary y-axis) by CLASS-CTEM for the 1851-2015 period in the transient historical simulation.

Deleted: 6

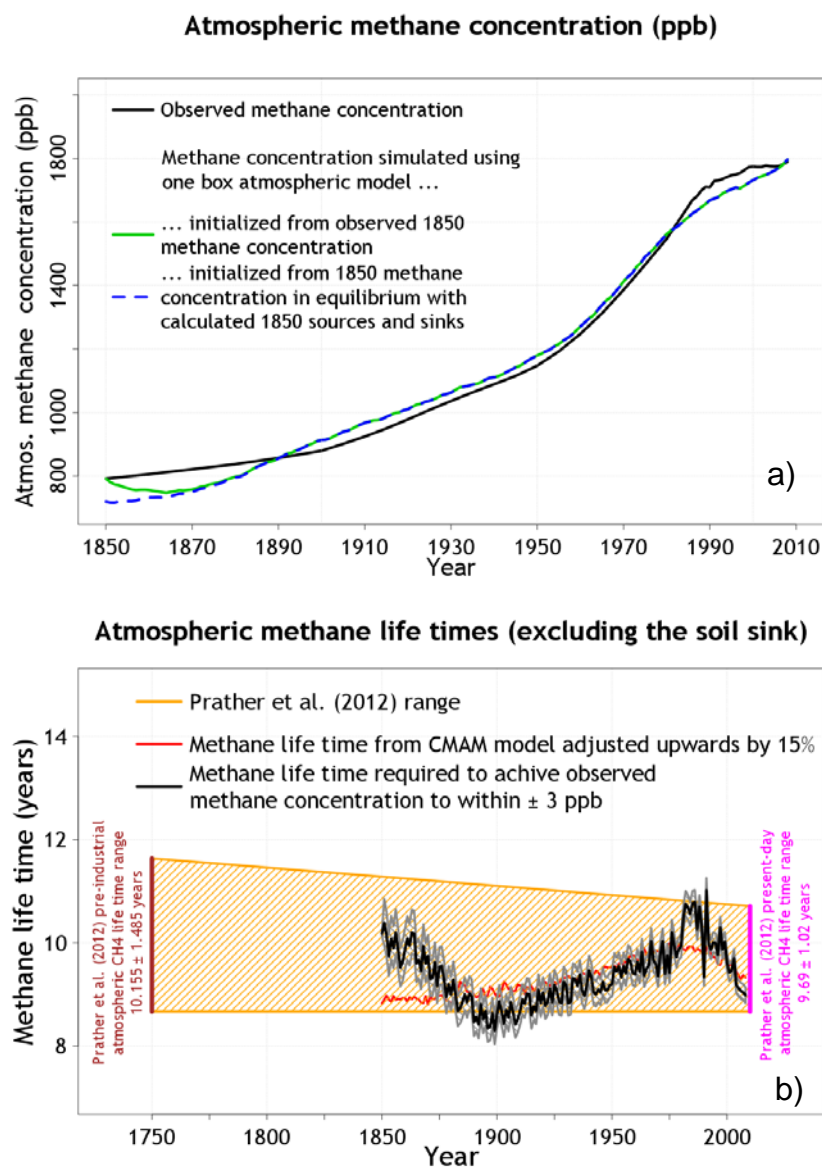


Figure 4: Comparison of simulated methane concentration over the historical period with its observation-based estimates (panel a). The simulation may be initialized from the 1850 observed methane concentration (solid green line) or from an 1850 concentration that is in equilibrium with 1850 specified methane sources and sinks (dashed blue line) as explained in section 3.2. Panel (b) compares the methane lifetimes required to achieve the observed increase in methane concentration over the historical period (black line) to within ± 3 ppb (shaded area between grey lines) with observation-based estimate of atmospheric methane lifetime based on Prather et al. (2012) and the adjusted atmospheric methane lifetime from CMAM.

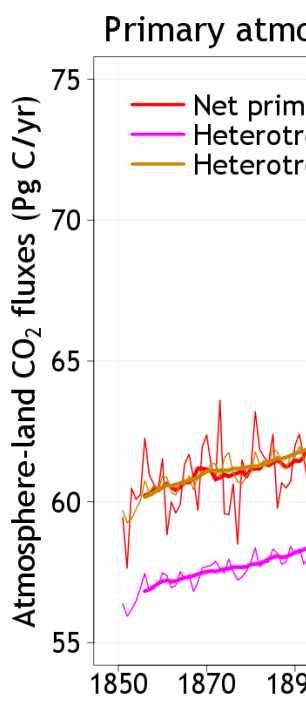


Figure 7: Time evolution of simulated net primary productivity (NPP) and heterotrophic respiration in the historical simulation both of which increase in response to increase in atmospheric CO_2 concentration. The thin lines show annual values while the thick lines represent the 10-year moving average. When fire CO_2 emissions are added to heterotrophic respiration the total amount is equal to Net primary productivity (NPP) - heterotrophic respiration - fire emissions) is near zero. Later in the 20th century and early 21st century, NPP is greater than the sum of heterotrophic respiration and fire CO_2 emissions, which creates the sink over land that is currently observed.

Figure 8: Comparison of global area burned from the transient 1851-2015 historical simulation (dark yellow line). The thick dark yellow line is the 10-year moving average.

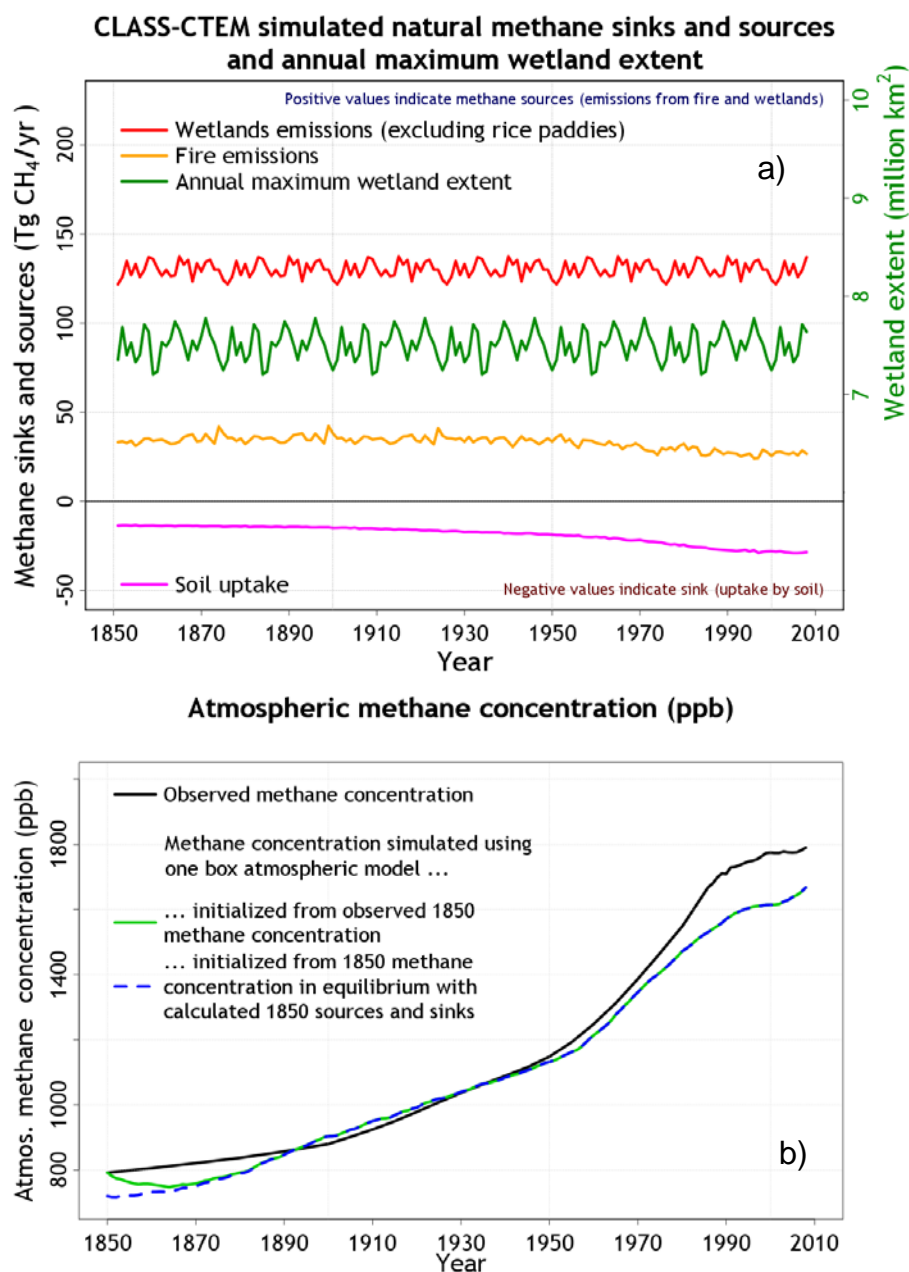
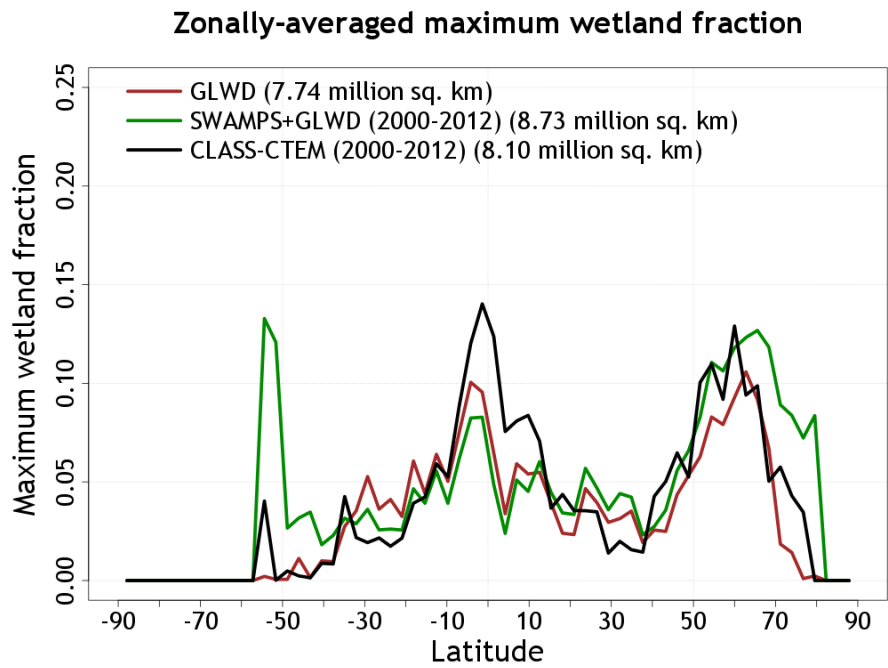


Figure 5: Time evolution of simulated natural methane fluxes (shown on the primary y-axis) and annual maximum wetland extent (shown on the secondary y-axis) by CLASS-CTEM for the 1851-2008 period for the case when wetland extent and methane emissions are not allowed to respond to changing climate and increase atmospheric CO₂ over the historical period (panel a). Panel (b) shows the simulated methane concentration over the historical period, together with its observation-based values, when the natural fluxes shown in panel (a) are used within the framework of the one box model of atmospheric methane.

Deleted: 10

1989
1990



1991

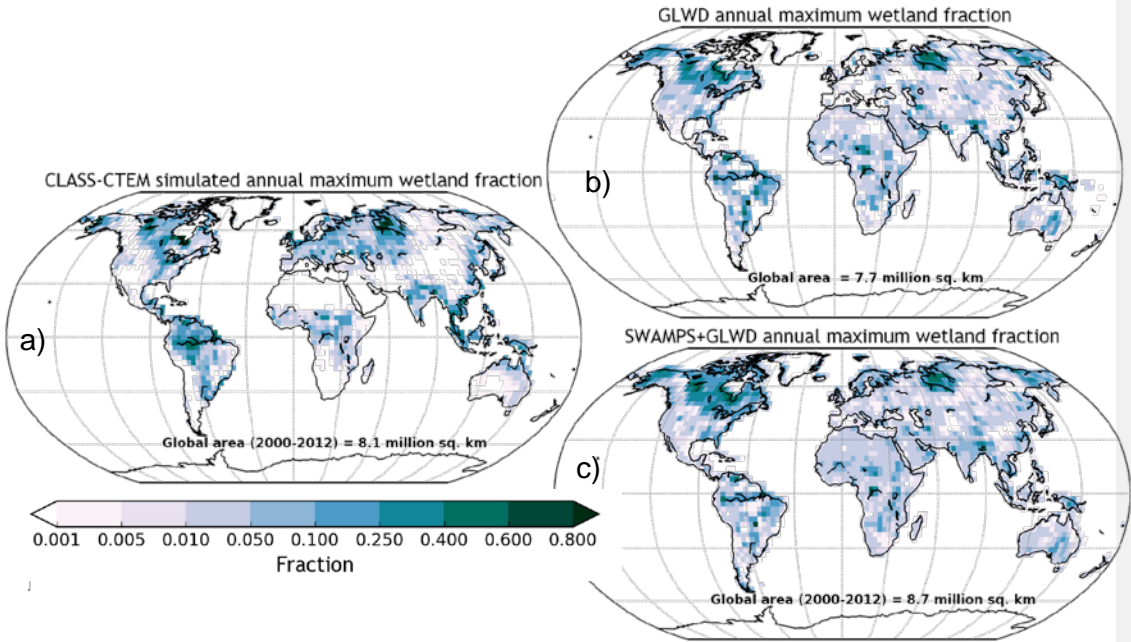
1992 | Figure 6: Comparison of simulated zonally-averaged maximum wetland fraction over land
1993 with observation-based estimates based on the Global Lakes and Wetland (GLWD; Lehner
1994 and Döll, 2004) and a new product that is formed by merging remote sensing based
1995 observations of daily surface inundation from the Surface Water Microwave Product Series
1996 (SWAMPS; Schroeder et al., 2015) with the static inventory of wetland area from the GLWD
1997 as explained in Poulter et al. (2017).

Deleted: 11

Field Code Changed

1998
1999
2000
2001
2002
2003
2004

2006
2007
2008



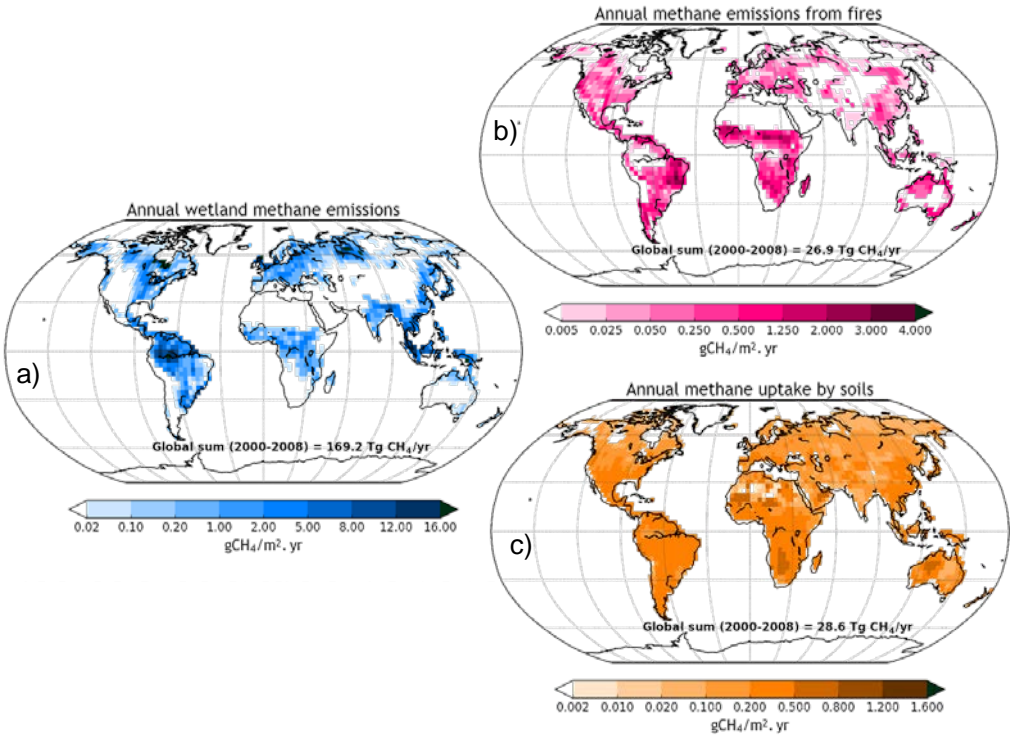
2009 | Figure 7: Comparison of geographical distribution simulated annual maximum wetland
2010 fraction with observation-based estimates based on the Global Lakes and Wetland (GLWD;
2011 Lehner and Döll, 2004) and a new product that is formed by merging remote sensing based
2012 observations of daily surface inundation from the Surface Water Microwave Product Series
2013 (SWAMPS; Schroeder et al., 2015) with the static inventory of wetland area from the GLWD
2014 as explained in Poulter et al. (2017).

Deleted: 12

Field Code Changed

2015
2016
2017
2018
2019

2021
2022
2023
2024
2025
2026
2027

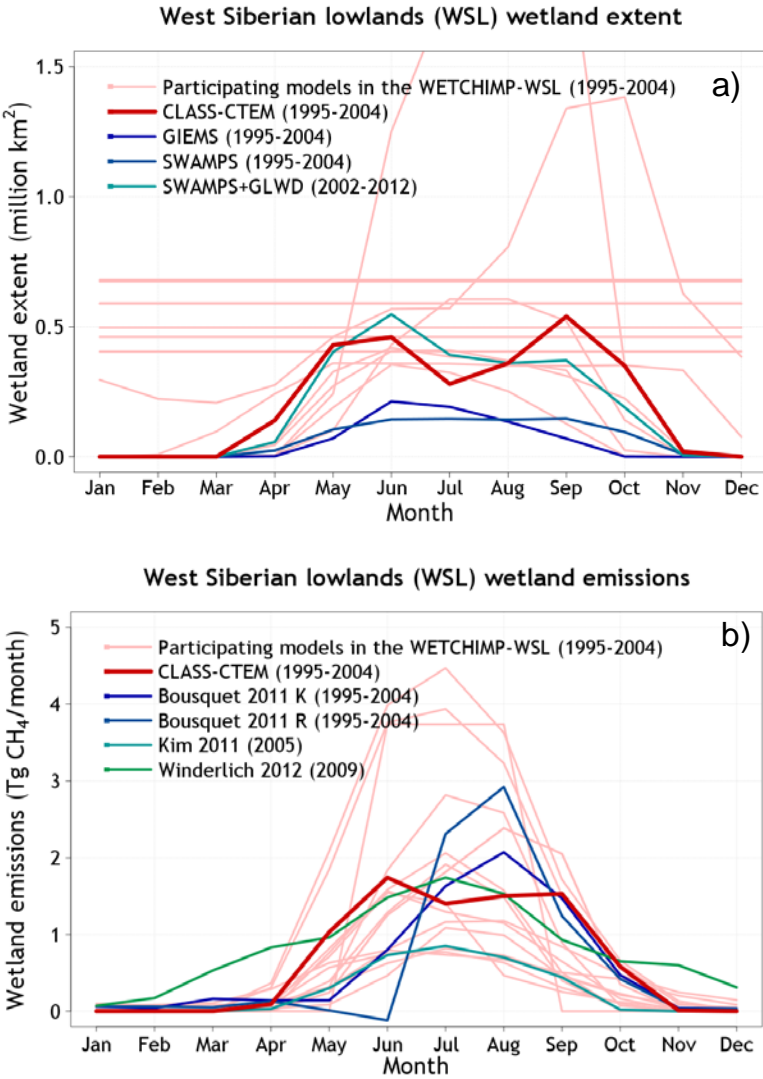


2028
2029
2030
2031
2032
2033

Figure 8: Geographical distribution of annual emissions from wetlands (panel a) and fire (panel c), and the soil sink (panel b) simulated by the CLASS-CTEM model. The data are averaged over the 2000-2009 period.

Deleted: 13

2035



2036

2037 | Figure 9: Comparison of CLASS-CTEM simulated wetland extend (panel a) and wetland
2038 methane emissions (pane; b) over the West Siberian lowlands (WSL) region with those from
2039 models participating in the WETCHIMP-WSL intercomparison and observation- and
2040 inversion-based estimates as discussed in section 3.5.

Deleted: 14

2041

2042

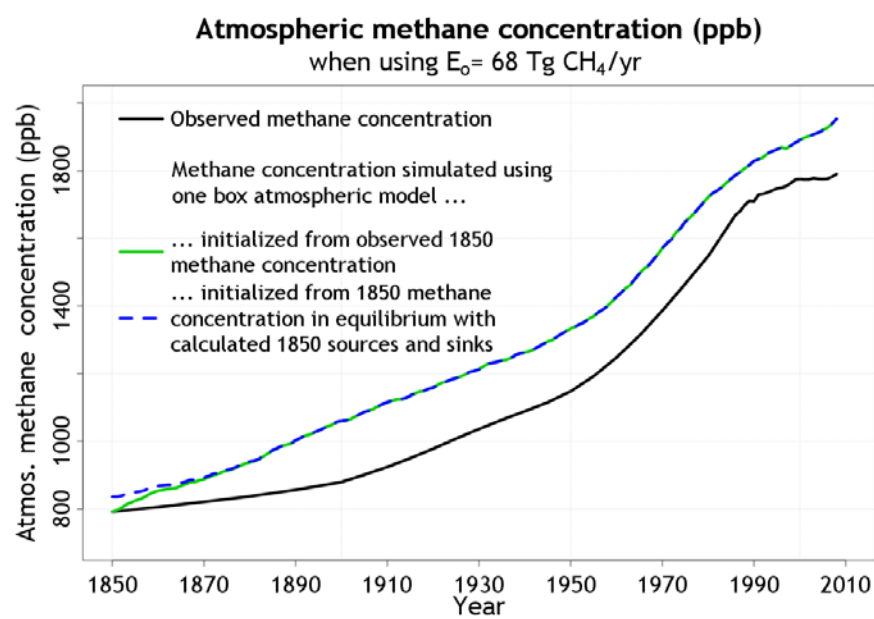
2043

2044

2046

2047

2048



2049

2050

2051

2052

2053

Figure 1Q: Simulated methane concentration over the historical period, together with its observation-based values, when other non-wetland natural methane emissions (E_o) are specified at $68 \text{ Tg CH}_4/\text{yr}$ over the historical period.

Deleted: 5

Appendix A: Calculation of wetland extent

Formatted: Font: Bold

Moved (insertion) [2]

Deleted: 2.1.1.1 Wetland extent¶

The distribution of wetlands is based on a simple formulation which takes into account the topography in a grid cell and its simulated grid-averaged soil moisture content similar to Kaplan (2002). The ETOPO1 digital elevation data (Amante and Eakins, 2009) are used to calculate slopes at 1 arc minute (1/60th degree) resolution. Each 1 arc minute grid cell is assigned a slope that is the average of eight slopes based on its elevation and the elevation of its eight surrounding grid cells. The objective is to find what fraction of a grid cell, at some given resolution, has slopes flatter than a given slope threshold. Figure A1 displays the fraction of each 0.5 degree grid cell with slopes less than the threshold of 0.002 (i.e. 0.2% slope) calculated using 1 arc minute slopes, hereafter referred to as the “flat” fraction of a grid cell (f_s). The flat fraction of grid cell is also shown at the current operational 2.81° resolution of CanESM4.2, which is the spatial resolution we have used in this study. Figure 1 shows that the approach is able to identify the flat regions of the world including the West Siberian and Hudson Bay lowlands, parts of northern Africa and in South America the Pantanal and the region bordering Argentina, Paraguay and Uruguay.

The flat fraction is the maximum fraction of a grid cell that can potentially become a wetland, if soils are sufficiently wet, and thus a source of CH₄ emissions. As the grid-averaged simulated soil wetness (w) of the top soil layer increases, above a given lower threshold (w_{low}) in a grid cell, its wetland fraction (f_w) is assumed to increase linearly until some specified higher soil wetness threshold (w_{high}) up to a maximum value equal to the flat fraction (f_s) in a grid cell.

$$f_w = \max \left(0, \min \left(f_s, \left(\frac{w - w_{low}}{w_{high} - w_{low}} \right) f_s \right) \right) \quad (A1)$$

2082

2083

Soil wetness ($w = \frac{\theta_l}{\theta_p}$) itself is defined as the ratio of volumetric liquid soil moisture content

2084

(θ_l) to the soil porosity (θ_p) for the top soil layer. The remaining fraction of the grid cell

2085

($1 - f_w$) is considered as the upland fraction. As simulated liquid soil moisture in the top soil

2086

layer responds to changes in environmental conditions the dynamic wetlands expand and

2087

contract. The upper and lower soil wetness thresholds are summarized in Table A1 and

2088

adapted to yield realistic geographical and latitudinal distribution of wetland extent compared

2089

to observation-based estimates.

2090

2091

Grid cell fraction with slope < 0.2% which can potentially become a wetland, climate permitting

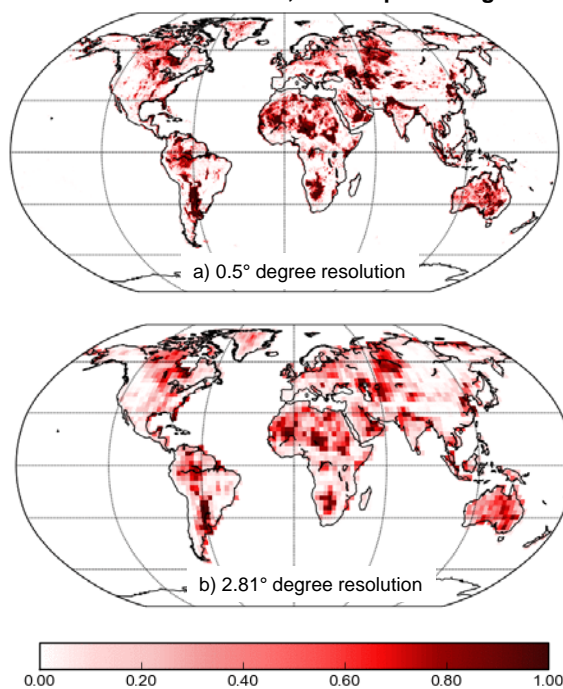


Figure A1: Fraction of grid cell with slopes less than the threshold of 0.002 (i.e. 0.2% slope) at a) 0.5° and b) 2.81° spatial resolutions, respectively.

Table A1: The upper and lower soil wetness thresholds for three latitudinal bands used in equation (1) to determine fractional wetland coverage in a given grid cell.

	<u>Latitudinal band</u>		
	<u>40°N to 90°N</u>	<u>35°S to 40°N</u>	<u>90°S to 35°S</u>
w_{low}	<u>0.45</u>	<u>0.55</u>	<u>0.70</u>
w_{high}	<u>0.90</u>	<u>0.99</u>	<u>0.99</u>

Appendix B: Driving data

Formatted: Font: Bold

Deleted: ¶
Page Break

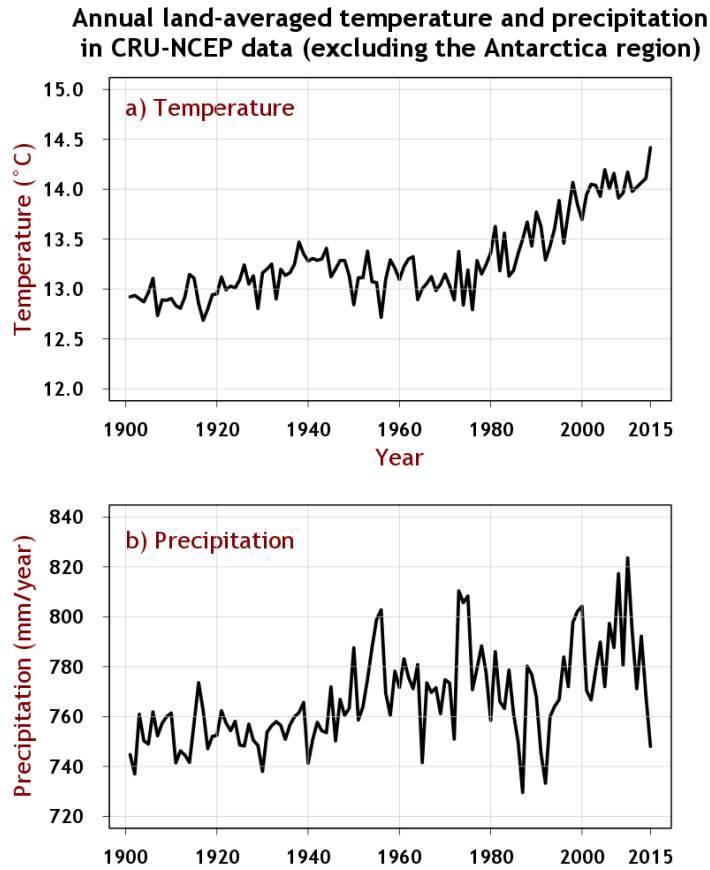


Figure B1: Annual land-averaged temperature and precipitation in version 7 of the CRU-NCEP data for the period 1901-2015, excluding the Antarctica region, that are used to drive the CLASS-CTEM model.

Globally-averaged CO₂ and CH₄ concentrations used to drive the CLASS-CTEM model

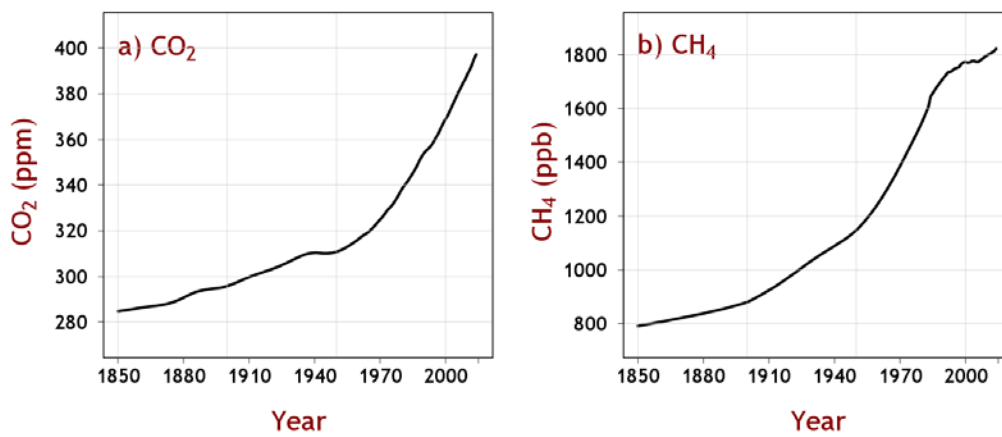


Figure B2: Globally-averaged CO₂ and CH₄ concentrations used to drive the CLASS-CTEM model.

Appendix C: Selected model results used to interpret methane emissions from wetland and fire.

Moved (insertion) [5]

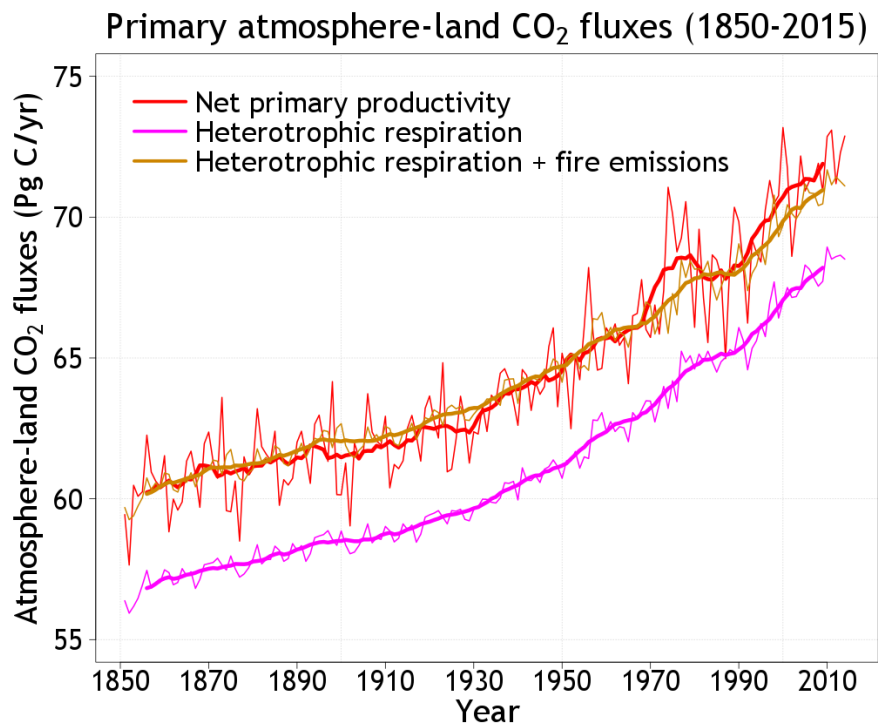
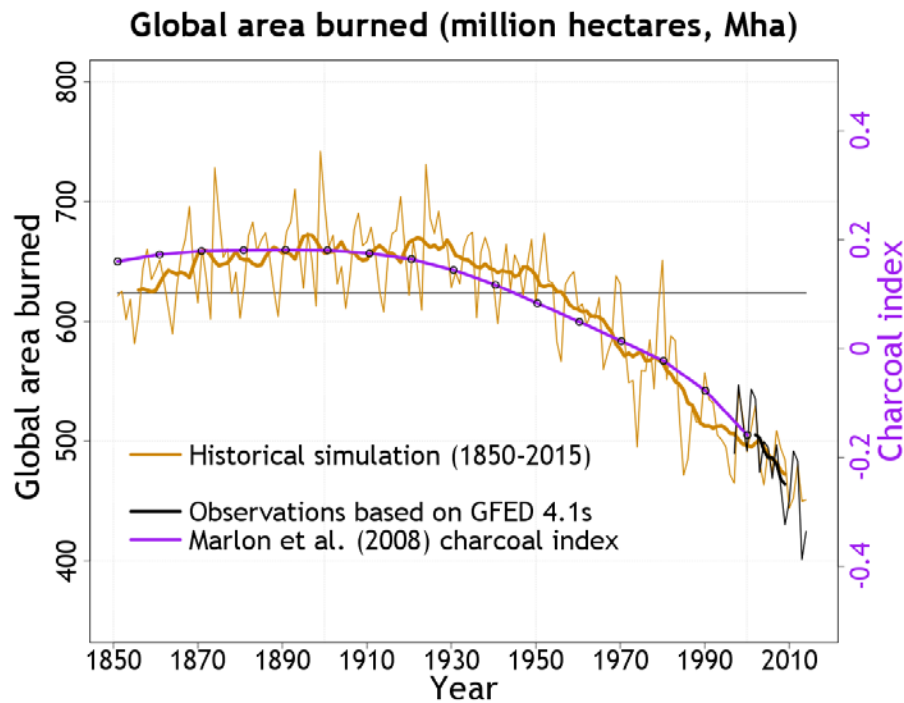


Figure C1: Time evolution of simulated net primary productivity (NPP) and heterotrophic respiration in the historical simulation both of which increase in response to increase in atmospheric CO₂ concentration. The thin lines show annual values while the thick lines represent their 10-year moving average. When fire CO₂ emissions are added to heterotrophic respiration the total amount is equal to NPP especially during 1850s as the case should be when the system is in equilibrium and net atmosphere-land CO₂ flux (equal to NPP – heterotrophic respiration – fire emissions) is near zero. Later in the 20th century and early 21st century, NPP is greater than the sum of heterotrophic respiration and fire CO₂ emissions, which creates the sink over land that is currently observed.

Deleted: 7

2145
2146
2147



2148
2149
2150
2151
2152
2153
2154
2155

Figure C2: Comparison of global area burned from the transient 1851-2015 historical simulation (dark yellow line). The thick dark yellow line is the 10-year moving average. Observation-based area burned (black line) are based on the GFED 4.1s data set. Model results are also compared to decadal charcoal index from version 3 of the Global Charcoal Database (purple line). Charcoal index is a proxy for burning and not for area burned per se and therefore only provides a qualitative measure.

Deleted: 8